Methodology Development of a Seam Weld Fatigue Analysis



Santiago Idarraga Saa Politecnico di Torino

For the Degree of Master's in Automotive Engineering

Supervisors

Prof. Carlo Rosso

Prof. Cristina Delprete

Contents

Introduction	1
Theory Background	3
Welding Techniques in the Automotive Industry	3
Resistance Spot Welding (RSW):	3
Resistance Seam Welding (RSEW):	4
Laser Beam Welding (LBW):	4
Arc Welding Processes (MIG/MAG, TIG/GTAW):	5
Friction Stir Welding (FSW):	6
Hot Spot Stress Concept and Design Stress	8
Dang Van Fatigue Criterion	10
Meshing Methodology in the Fayard Approach	12
Element Sizing at the Weld Intersection:	12
Simulation of Weld Rigidity with Rigid Elements:	13
Mesh Gradation:	14
Tests	16
Loading Configurations	18
Test Output and Data Handling	19
Calculations	19
Axial Load (X-axis):	19
Offset Load (Y-axis):	20
Four-Point Bending (Z-axis):	21
FEM analysis	24
Validation with Different Joint Configurations	26
SN Curve with Weibull Distribution	29
Simulation Procedure for OptiStruct and Abaqus	31
Process automation:	32
Conclusion	35
Main Findings:	35
Correlation between Simulations and Experiments:	35
Performance of the Equivalent Stress (τ_o):	35
Recommendations for Improved Correlation:	35

	Validation of Fayard's Methodology:	36
	Practical Implementation:	
	Automation through Plugin Development:	
	Final Remarks:	37
	Further work:	37
Ref	erences	38
Anı	nexes	40
(Optistruct	40
A	Abagus	46

Table Of Figures

Figure 1. Spot Welding Diagram. [8]	3
Figure 2. Resistance Seam Welding Diagram [10]	4
Figure 3. Laser Beam Welding Diagram [13]	5
Figure 4. TIG and MIG Welding Diagram [15]	6
Figure 5. Friction Stir Welding Diagram [17]	7
Figure 6. Welding Processes Summary	8
Figure 7. Representation of the Hot Spot Stress and Non-Linear Stress near a weld	9
Figure 8. Fayard Meshing rules for a lap weld joint	13
Figure 9. Fayard Meshing rules for a T-joint	14
Figure 10. Mean fatigue strength at 10^6 cycles obtain from Fayard lab tests[1]	16
Figure 11. Dimensions for the Fx and Fy test probes	17
Figure 12. Dimensions for the four point bending (Fz) test	17
Figure 13. Lap weld lateral view	18
Figure 14. Stress Representation during the Fx Test	20
Figure 15. Stress Representation during the Fy Test	20
Figure 16. Load Representation during the Fz Test	21
Figure 17. Individual SN curves from the three Lap Weld Tests	22
Figure 18. SN curved from the combined data of the Tests	23
Figure 19. Comparison between the normalized stresses of theory and simulation	24
Figure 20. SN curve using Dang Van's Equivalent Stress	
Figure 21. T-joint weld lateral view	26
Figure 22. SN curve derived from lap weld tests and values of the T-Joint Tests	28
Figure 23. Tau-N curve derived from lap weld tests and values of the T-Joint Tests	28
Figure 24. Weibull Tau-N curve derived from lap weld tests and values of the T-Joint Tests	30
Figure 25. Overall workflow of the methodology	32
Figure 26. Fayard Builder Plugin with its two main inputs	33
Figure 27. Fayard Post processing plugin.	34

Acknowledgments

I would like to thank Professor Carlo Rosso and the Engineers Pasquale Iacobone and Domenico Macri for allowing me to undertake this project and for giving me guidance during its process.

Last, but not least. I would like to thank my family and friends for having the patience to bear with me and for all the support they have given me.

Abstract

This thesis presents a comprehensive study on the fatigue behavior of thin-sheet steel structures joined by seam welds, combining experimental testing and finite element (FE) simulations based on the meshing and fatigue evaluation methodology proposed by Fayard et al. The primary objective was to establish a reliable and practical workflow for the fatigue assessment of welded joints using conventional FE software—Abaqus and OptiStruct—without requiring specialized fatigue analysis packages.

Experimental tests were performed on lap-jointed specimens made of 2 mm thick, 50 ksi steel plates welded using the GMAW-P process. The resulting force—cycle (F—N) data were converted into stress—cycle (S—N) curves using both maximum principal stress and an equivalent stress parameter derived from the Dang Van multiaxial criterion. These curves were then used to predict the fatigue life of T-joint specimens subjected to multiple loading conditions (Fx, Fy, and Fz). A strong correlation was observed between experimental and simulated fatigue lives, particularly when using the maximum principal stress, confirming the robustness of Fayard's meshing approach and fatigue model for thin-sheet welded structures.

To improve modeling efficiency, two Python-based plugins were developed for Abaqus: one automates mesh generation and weld element creation following Fayard's rules, while the other performs post-processing to calculate equivalent stresses and estimated fatigue lives. These tools significantly reduce manual effort and increase consistency in fatigue evaluations. Overall, this study demonstrates that accurate and efficient fatigue assessment of seam-welded structures can be achieved using standard FE tools enhanced by automated modeling and analysis routines.

Introduction

Seam-welded joints are widely used in thin-walled steel structures in the automotive industry due to their manufacturability, cost-efficiency, and structural performance. However, their fatigue behavior under dynamic loading remains a critical concern in vehicle design, especially as components are subjected to a combination of tensile, bending, and vibrational loads over service life. Accurate fatigue prediction of such assemblies is essential to ensure safety, durability, and compliance with industry standards.

Traditionally, fatigue assessment in finite element analysis of welded structures has relied on dedicated modelling techniques involving shell elements for base materials and 1D elements for welds. Stress tensors are typically extracted at critical locations such as the weld toe, and fatigue criteria like the Dang Van maximum shear method are applied to evaluate crack initiation potential [1,2]. These approaches have been validated through extensive fatigue test campaigns using various weld configurations and load cases. In addition, recent IIW guidelines have proposed shell element-based weld models for evaluating weld root fatigue, showing promising results in correlating numerical predictions with experimental data [3–5].

However, using fatigue-specific software packages such as FE-Safe or integrated fatigue solvers often requires additional computational resources and expertise, which may not be practical during early-stage design or large-scale analyses. In this context, the Fayard method offers an attractive alternative. Developed for polycyclic fatigue design of welded structures, it enables stress-based fatigue evaluation using standard FEM tools, without requiring fatigue-specific modules, while still achieving high correlation with experimental outcomes [1,2].

This thesis was carried out in collaboration with Stellantis, to define a simple and reliable simulation methodology to represent the dynamic behavior of seam welds, using only conventional FE software—Abaqus and OptiStruct (Nastran). The project aims to develop a standardized workflow for modelling seam-welded joints, including model setup, material card definition, boundary conditions, and stress extraction recommendations. This workflow is intended to serve as a reference for similar applications in the future.

To this end, the Fayard methodology was selected due to its simplicity, adaptability, and demonstrated accuracy in previous studies [1,2]. It supports using common modelling techniques (e.g., shell or solid elements) to represent welded joints, and relies on stress-based evaluation criteria that do not depend on dedicated fatigue tools. This approach suits industrial environments where efficiency and reproducibility are key.

Experimental validation was performed using lap-jointed specimens with single-sided seam welds, subjected to three different loading conditions: axial, offset (parallel to weld), and four-point bending. The tests produced force-cycle (F–N) data, from which stress-cycle (S–N) curves were derived using theoretical stress calculations that accounted for bending, eccentricity, and stress concentration. These were then compared to the maximum principal stresses obtained from FEM simulations built according to the Fayard method. Results showed strong agreement between theoretical and simulated stress values, indicating that the method accurately captures the load transmission and stress distribution in the weld region. Minor discrepancies are attributed to residual stresses from welding, geometric variability in the welds, surface conditions, and material heterogeneity.

Finally, recognizing the time-consuming and error-prone nature of manually building FEM models following Fayard's rules, this work also introduces two custom-developed Python plugins for Abaqus. The first automates the meshing and creation of rigid elements that simulate weld connections, based on user-selected geometric references and weld leg size. The second automates post-processing, extracting stresses from FEM results to compute the equivalent stress (τ_0) and fatigue life (N) using the derived S–N curves. These tools greatly reduce modeling time and improve reproducibility, making the Fayard methodology more practical for large or complex structures. Together, they represent a step toward the industrial digitalization and automation of fatigue assessment for welded thin-sheet structures.

Theory Background

Welding Techniques in the Automotive Industry

Within the automotive industry's manufacturing processes, welding technologies play a fundamental role in the construction of vehicle structures. The development of different automobile configurations has led to the need to create and apply different welding methods that are appropriate for the area and purpose of the parts being joined. The increasing complexity of designs seeking to reduce weight and the use of different materials that have increased structural rigidity have exponentially encouraged improvements in the quality of joints to withstand static and dynamic loads. Below are some of the most common welding methods used during vehicle manufacturing.

Resistance Spot Welding (RSW):

This is one of the most prevalent methods in vehicle bodies, with approximately 4500 spot weld joints [6] used. This welding is generated from the heat created by the resistance of metals when an electric current passes between two copper electrodes through the parts to be welded. Because of this, metals with higher resistivity, such as steel, are easier to weld by this method than other metals, such as Aluminum, whose conductivity is higher [7].

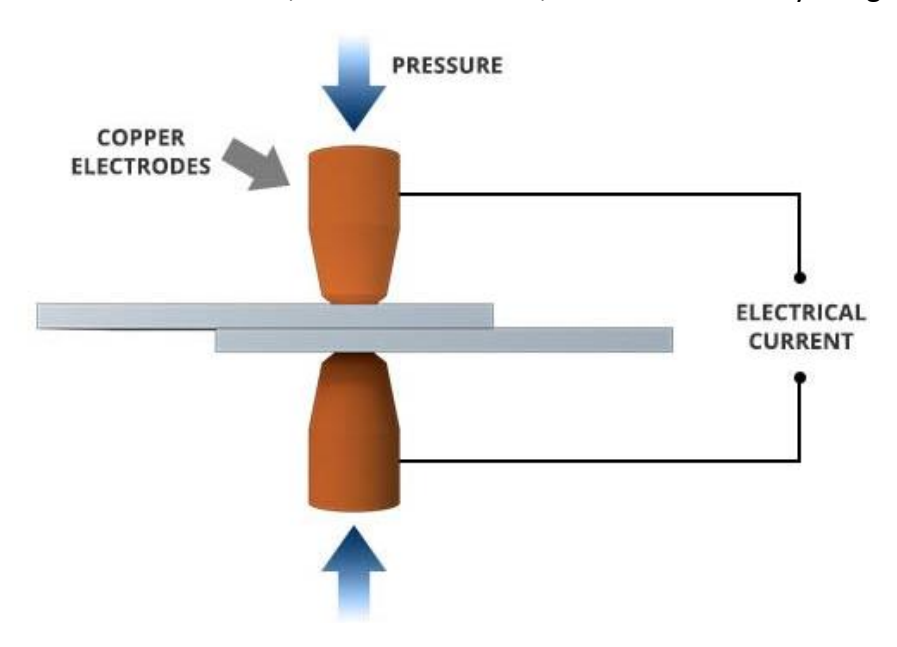


Figure 1. Spot Welding Diagram. [8]

This is a process that works very well for thin sheets, such as those used in the automotive industry for body components. Furthermore, its self-clamping structure facilitates the use of robotics in the manufacturing process, increasing factory productivity while maintaining standard quality.

Resistance Seam Welding (RSEW):

Following the same principle used in RSW, Resistance Seam Welding uses wheel-shaped electrodes rolled along the joint. These electrodes can generate a continuous or intermittent current to produce a series of spots close enough to create a continuous weld [9]. This process is ideal for components that require a seal against gases or liquids, such as fuel tanks, mufflers, or battery enclosures. However, it requires a more complex system to maintain all parameters at correct levels, such as electrode pressure and proper current overlap.

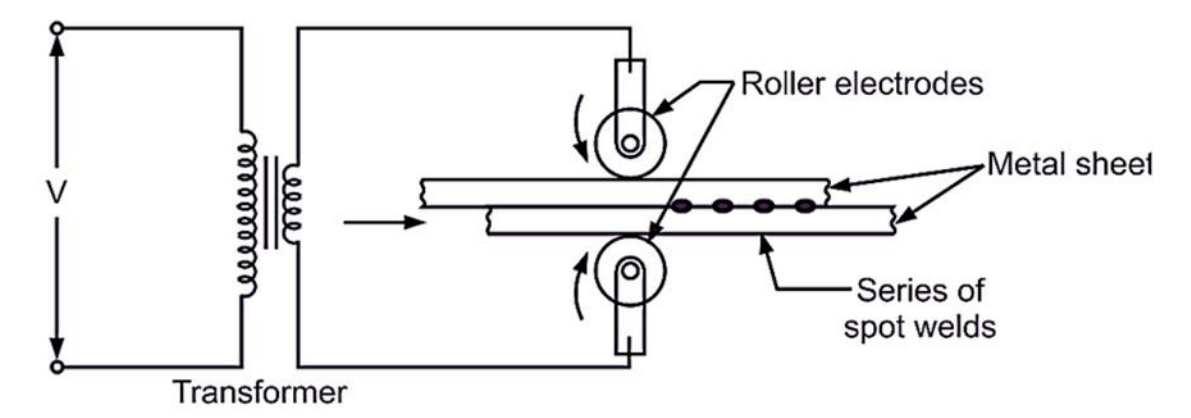


Figure 2. Resistance Seam Welding Diagram [10]

Laser Beam Welding (LBW):

As its name suggests, this method uses a high-power concentrated light source to melt and fuse materials, often with high penetration and high speed. This type of welding usually provides a high-power density of energy for melting and concentrates the heat in a small area, with a very narrow heat-affected zone [11]. In the automotive industry, high-power CO2 lasers (output powers up to 60 kW) are used for gears and transmission components. Neodymium lasers with optical-fiber delivery have a lower output power, ranging from 3 to 5 kW. Still, they are ideal for use during the assembly of body-in-white parts [12] as these parts are thin enough, around 0.5 and 5 mm thick, to achieve fusion.

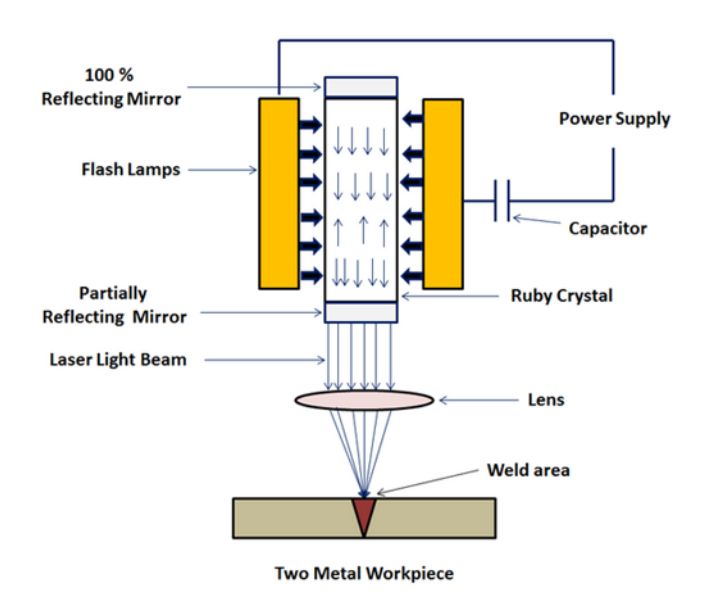


Figure 3. Laser Beam Welding Diagram [13]

In addition to being used in high-volume applications by being able to be installed in different areas of the production line, and also integrating with automated systems and robots, the LBW has the versatility to be used with different types of materials, including carbon steels, HSLA steels, stainless steel, aluminum, and titanium.

Arc Welding Processes (MIG/MAG, TIG/GTAW):

Being among the most widely recognized methods, both arc welding processes play a crucial role in the automotive industry, used extensively for both vehicle fabrication and repair. MIG welding uses a continuous consumable wire electrode that is melted by an automatic or semi-automatic electric arc [14]. This system is shielded by a gas atmosphere, usually inert gases like argon or helium, or active gases like CO2 or argon and CO2 mixtures. Often, this process offers high productivity and easy automation, which is ideal for chassis structures, subframes, exhaust systems, and suspension components, especially in robotic production lines. On the other hand, in TIG welding, the electrode is a non-consumable tungsten electrode used alongside a separate consumable filler material with an inert shielding gas [14]. This configuration makes the process slower; however, it is more precise and produces a superior weld quality, making it ideal for thin materials and high-performance parts such as aluminium fuel tanks, stainless-steel exhausts, and electric vehicle battery enclosures.

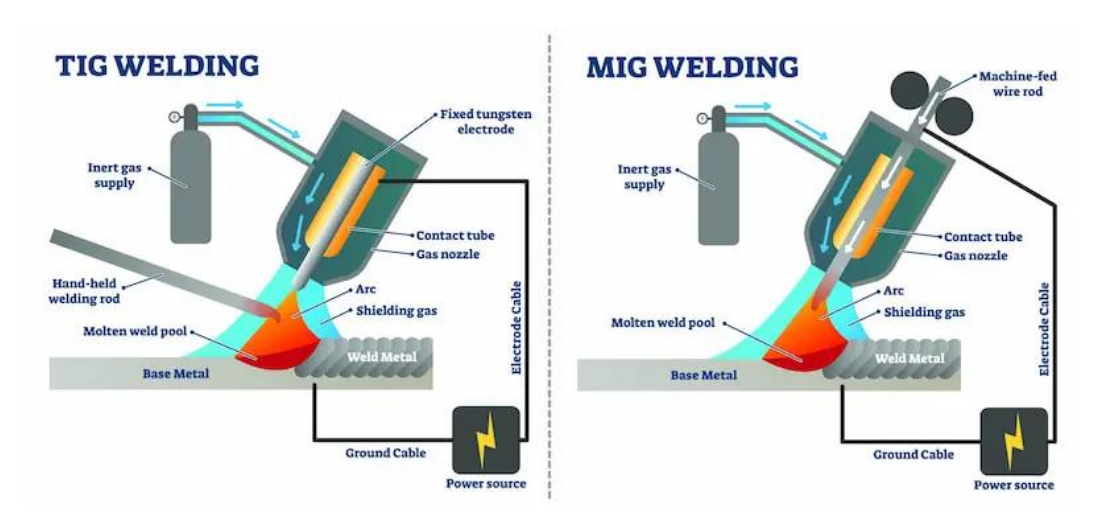


Figure 4. TIG and MIG Welding Diagram [15]

Friction Stir Welding (FSW):

During this method, the heat required for bonding is generated by mechanical friction between two surfaces under controlled pressure, rather than by melting the materials [16]. This allows metals and alloys to be joined without reaching their fusion temperature, resulting in defect-free, high-strength joints with minimal distortion. In the automotive industry, friction welding is widely used for connecting dissimilar materials and rotational components, such as drive shafts, engine valves, gear parts, and steering columns, where reliability is critical. FSW uses a non-consumable rotating tool to plastically deform and mix the material along the joint line, producing a continuous, solid-phase seam. FSW is increasingly used in lightweight aluminium structures, EV battery enclosures, and body panels. This method has become useful for joining aluminium to steel and other difficult combinations, necessary for multi-material and lightweight designs.

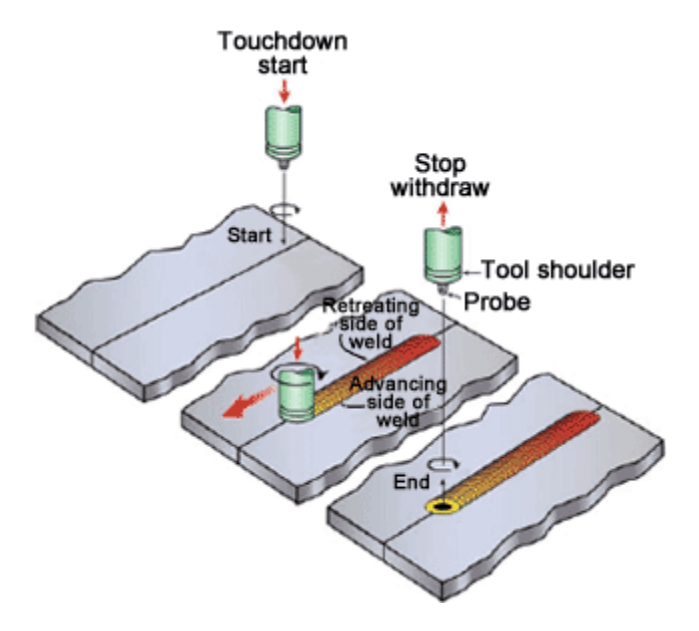


Figure 5. Friction Stir Welding Diagram [17]

Figure 6 summarizes the main characteristics of the most commonly used methods in the automotive industry. The table highlights key aspects such as process type, materials, applications, advantages, and limitations, providing a comparative overview of techniques ranging from traditional resistance-based welding to advanced laser and friction-based processes.

Welding	Process Type	Typical	Automotive	Main	Main
Process		Materials	Applications	Advantages	Limitations
Resistance	Fusion,	Mild steel,	Body-in-	High speed,	Produces
Spot Welding	resistance-	high-strength	white (BIW),	easily	discrete
(RSW)	based	steel	door panels,	automated,	welds (not
			brackets	low cost per	continuous),
				joint	limited to
					sheet
					materials
Resistance	Fusion,	Low-carbon	Fuel tanks,	Produces	Limited to
Seam	resistance-	steel,	exhaust	leak-tight,	overlap joints
Welding	based	stainless	systems,	continuous	and thin
(RSEW)	(continuous)	steel,	transmission	seams; easily	sheets;
		aluminium	housings,	automated	requires
			sealed		precise
			components		control
Arc Welding	Fusion,	Carbon	Chassis,	Versatile,	High heat
(MIG/MAG,	electric arc	steels,	subframes,	strong joints,	input causes
TIG)			suspension		distortion;

		aluminium, stainless steel	arms, exhaust systems	suitable for thick sections	slower than resistance methods
Laser Welding (LBW)	Fusion, energy beam	High-strength steels, aluminium alloys	Roof seams, doors, tailored blanks, EV battery trays	Deep penetration, minimal distortion, high speed	Expensive equipment, tight fit-up tolerances
Friction- Based Welding (FSW, Rotary, Linear)	Solid-state (no melting)	Aluminium, magnesium, steel– aluminium combinations	EV battery housings, drive shafts, lightweight panels	No melting. Low distortion, strong joints, joins dissimilar metals	Limited geometry; slower than RSW or LBW

Figure 6. Welding Processes Summary

Although a wide variety of welding processes are employed in the automotive industry, such as resistance spot welding, arc welding, laser welding, and friction-based techniques, each selected according to specific material and design requirements, the present study focuses on continuous seam welds. Seam welding processes create continuous or overlapping joints that ensure structural continuity and leak-tightness, which are essential in components subjected to dynamic loads, such as fuel tanks, exhaust systems, and body structures. Because these joints often experience complex stress distributions and fatigue loading, their accurate analysis and numerical simulation have become increasingly important for predicting performance and improving design reliability. Accordingly, this work emphasizes the mechanical behavior and durability assessment of seam welds, providing a foundation for understanding their role in modern automotive engineering.

Hot Spot Stress Concept and Design Stress

In the fatigue analysis of welded structures, particularly in thin-walled components subjected to cyclic loading, cracks commonly initiate at geometrically critical regions such as weld toes. These regions, due to their structural discontinuities and localized stress concentrations, are referred to as hot spots. Understanding and characterizing the stress state at these hot spots is essential for accurate fatigue life prediction and structural integrity assessments.

Radenkovic provided a foundational distinction between two categories of stresses in the vicinity of a hot spot: the actual local stress σ_l and the geometrical hot spot stress σ_{hs} [18]. As presented in Fig.1, the local stress σ_l incorporates the sharp increases caused by local phenomena such as weld toe geometry, surface roughness, welding defects, and undercuts,

which are highly irregular features and often difficult to model explicitly. This stress state governs the initiation phase of fatigue cracking but is notoriously challenging to evaluate either numerically or experimentally due to its randomness and sensitivity to microscale effects.

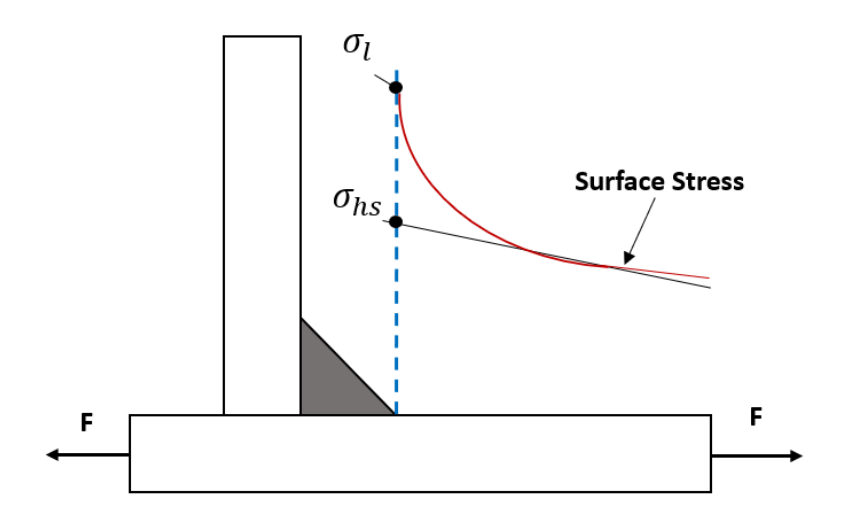


Figure 7. Representation of the Hot Spot Stress and Non-Linear Stress near a weld.

In contrast, the hot spot stress σ_{hs} excludes these highly localized effects and reflects the stress concentration due to structural geometry alone. It can be reliably estimated using finite element analysis (FEA), provided that appropriate mesh refinement and modelling techniques are used. Given the complexity of directly capturing σ_l , Radenkovic proposed the use of σ_{hs} as a surrogate for fatigue design, leading to the definition of the design stress.

This design stress serves as a standardized measure to represent the effective stress range responsible for fatigue damage under cyclic loading conditions. Fayard et al. (1996) built upon Radenkovic's framework by applying this concept specifically to continuously welded joints, such as those commonly found in the automotive, civil engineering, offshore, and rail industries [2]. Their approach assumes that arc-welded joints within a given manufacturing process are consistent in their local effects (due to repeatable weld geometry and similar defect profiles), thereby justifying the omission of explicitly modelling σ_l , .

This simplification enables a practical fatigue assessment strategy: by focusing on σ_{hs} , engineers can derive fatigue life predictions based on measurable and reproducible quantities from numerical simulations. It also facilitates the development of generalized design rules and methodologies, such as the one proposed by Fayard, that are suitable for

implementation in standard FEM software environments without requiring specialized local stress modelling.

Further clarification of the hot spot stress concept is provided by the International Institute of Welding (IIW), as summarized by Barsoum (2020). According to the IIW, the structural hot spot stress σ_{hs} includes all stress-raising effects from the structure itself but explicitly excludes the non-linear peak stress due to the local weld profile. In other words, the hot spot stress represents the macro-scale influence of the component's geometry and loading, separate from micro-scale weld toe effects[19].

The IIW approach is particularly applicable in cases where:

- (1) No clearly defined nominal stress exists due to complex geometry or loading conditions.
- (2) The structural detail cannot be easily categorized using standard fatigue detail classes.

To evaluate σ_{hs} , the IIW recommends using stress extrapolation methods. This involves extracting stress values at predefined reference points on the surface of the component, typically at distances of 0.4t and 1.0t from the weld toe (where t is the plate thickness), and extrapolating to estimate the structural stress at the weld toe itself. This method ensures consistent determination of the stress used in fatigue evaluation.

In situations involving biaxial stress states, the IIW suggests using the principal stress oriented within ±60° of the normal to the weld toe. This orientation is considered the most influential on fatigue crack initiation, as it aligns with the primary direction of crack propagation.

In summary, the hot spot stress concept forms a critical foundation for modern fatigue assessment of welded structures. It bridges the gap between inaccessible local stress effects and practical, simulation-based fatigue evaluation. This conceptual framework is central to the Fayard method and underpins its simplicity and robustness as an industrial design tool.

Dang Van Fatigue Criterion

Fatigue failure in welded structures is often driven by complex multiaxial stress states, where conventional uniaxial fatigue models fall short. The Dang Van criterion, proposed by Ky Dang Van, offers a robust multiaxial fatigue model based on the hypothesis that microplasticity initiates at the grain level due to localized stress fluctuations, even when the

global material response remains elastic [20]. This makes the criterion particularly suitable for high-cycle fatigue conditions typically observed in welded joints.

The Dang Van criterion postulates that fatigue failure can occur when, at any moment in the loading cycle, the shear stress $\tau(t)$ on a critical material plane, combined with the influence of the hydrostatic stress p(t), exceeds a material-dependent fatigue threshold. The condition is expressed as:

$$\tau(t) + \alpha * p(t) \le \tau_D \qquad \dots (1)$$

Where:

au(t): Instantaneous maximum shear stress on a material plane

p(t): Hydrostatic (mean) stress

 α : Material parameter related to sensitivity to hydrostatic stress

 τ_D : Fatigue limit in pure reversed torsion

Calculation of Stress Terms

To apply the Dang Van criterion in practice, it is essential to compute $\tau(t)$ and p(t) from the stress tensor at each integration point in the model. For linear elastic simulations, these values can be directly derived from the principal or Cartesian components of the stress tensor $\sigma(t)$.

1. Hydrostatic Stress p(t)

The hydrostatic stress is the mean normal stress at a given time:

$$p(t) = \frac{\sigma_x + \sigma_y + \sigma_z}{3} \qquad \dots (2)$$

In case of plane stress (i.e., in thin shell models), $\sigma_z = 0$.

2. Shear Stress $\tau(t)$

The instantaneous shear stress $\tau(t)$ used in the criterion corresponds to the maximum shear stress amplitude found on a material plane at time t. It can be computed as:

$$\tau(t) = \frac{\sigma_1 - \sigma_3}{2} \qquad \dots (3)$$

Where:

 σ_1 : maximum principal stress

σ_3 : minimum principal stress

This formula assumes that the maximum shear occurs on a plane where the difference between the principal stresses is greatest, which is consistent with the Tresca criterion for yielding. If stress states vary in time (i.e., under cyclic loading), $\tau(t)$ is tracked over time to find the maximum value during the cycle. And, as with the calculations of the hydrostatic stress, the formulation changes when dealing with plane stress, considering the minimum principal stress as σ_2 .

Meshing Methodology in the Fayard Approach

Fatigue analysis of continuously welded thin-shell structures in the automotive industry presents unique challenges due to geometry-induced stress concentrations at welded joints. A crucial step to ensure reliable simulation results, especially when using shell element models, is implementing an appropriate meshing strategy near weld intersections, where steep stress gradients often occur and fatigue cracks often initiate.

The Fayard methodology was originally developed for arc-welded thin-sheet structures to address these challenges. This is achieved through a set of meshing rules that allow for the accurate extraction of the design stress, defined as the geometrical stress amplitude at the weld toe or root [22]. These rules were established with two primary objectives: to correctly model the local stiffness introduced by the weld geometry and to accurately reproduce the stress transfer mechanism from one sheet to another through the weld [21,22,23].

In thin shell finite element models, plates are typically represented by their mean surfaces, which complicates the modeling of the physical intersection where sheets are joined. This intersection behaves as a localized three-dimensional region even though the global model is two-dimensional. Consequently, the stress distribution near the weld toe or root can be highly sensitive to the local mesh resolution [22]. To resolve this, Fayard and collaborators proposed a clear meshing methodology that standardizes how to discretize welded joints in shell models.

The key principles of this methodology are:

Element Sizing at the Weld Intersection:

The shell elements for analysis are located adjacent to the weld intersection and are defined with dimensions approximately equal to the weld toe length. This size selection reflects both the physical scale of the weld and the need to capture the high stress gradient near the toe without requiring excessively fine meshing. The maximum design stress is typically located at the centroid of the element, which corresponds to the weld toe and weld root location [22].

Simulation of Weld Rigidity with Rigid Elements:

Because the weld introduces additional local stiffness, it is essential to replicate this structural effect in the FEM model. This is achieved by inserting rigid elements (e.g., RBE2 elements in Nastran/Optistruct or coupling constraints in Abaqus) that connect the mean surfaces of the two shell parts being welded. These rigid links are defined by pairs of nodes placed at the mid-height of the weld leg, along the entire weld line. One node belongs to the shell mesh of the base plate and the other to the attached component [21,22]. This configuration simulates the mechanical continuity and load transfer across the weld zone.

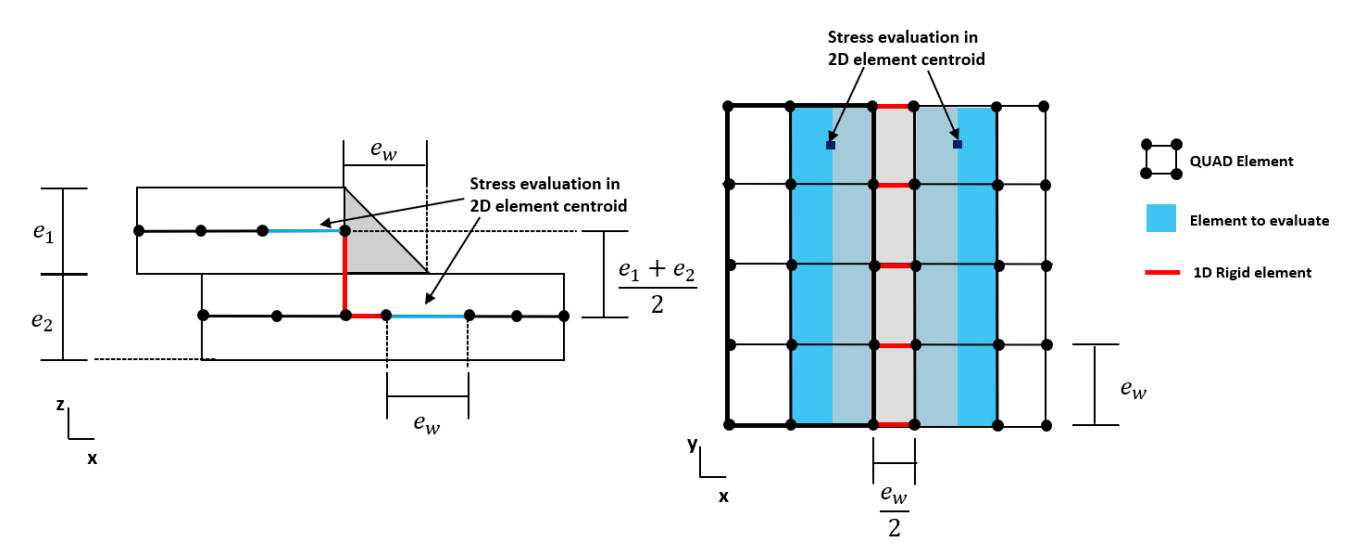


Figure 8. Fayard Meshing rules for a lap weld joint

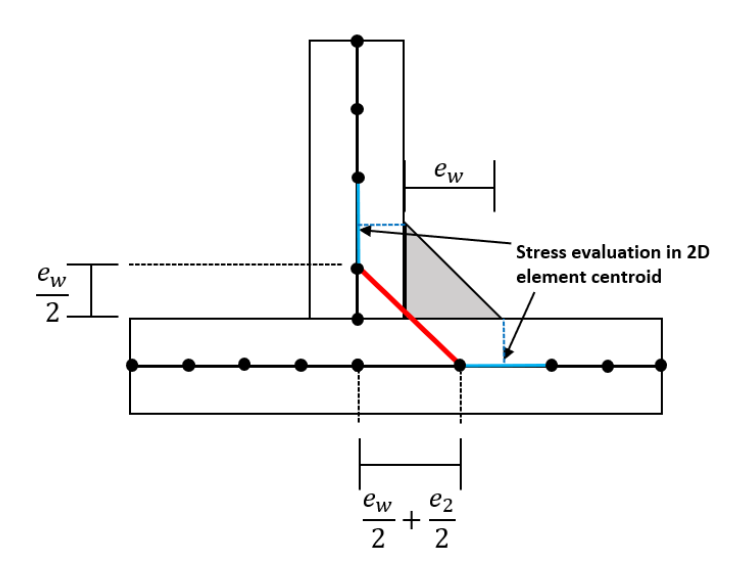


Figure 9. Fayard Meshing rules for a T-joint

Mesh Gradation:

Beyond the immediate intersection region, the mesh size gradually increases with distance from the weld. This ensures the model captures the necessary stress concentration near the weld while maintaining computational efficiency in less critical areas [22].

By adhering to these meshing rules, the simulation becomes capable of capturing the asymptotic mechanical field near the weld, i.e., the stress field that governs fatigue behavior, without the need for extremely fine meshes or the use of more complex modeling techniques such as solid elements or specialized weld modeling modules. Importantly, using this approach, the design stress extracted at the weld toe or root corresponds closely with experimental observations, enabling a direct correlation between numerical predictions and physical fatigue test data [23].

The overall benefit of this method is its practical applicability: it allows engineers to carry out fatigue life predictions in standard finite element environments (such as Abaqus or Nastran/Optistruct) using simple shell models, without resorting to additional software like FE-Safe or fatigue post-processors. As such, it aligns with the broader objective of developing efficient, simulation-ready workflows for fatigue assessment in industrial applications.

While the meshing rules defined by Fayard allow for accurate geometric stress calculation at hot spots in shell element models, they also provide a foundation for integrating multiaxial fatigue analysis. In real-world loading scenarios, welded joints are

often subjected to complex stress states, such as combinations of axial, bending, and torsional loads, which require fatigue criteria capable of capturing these effects. To address this, Fayard incorporated the Dang Van criterion into his methodology, enabling the use of a unified fatigue design curve for welded structures, regardless of geometry or loading mode.

In their study, Fayard performed extensive fatigue testing on elementary welded specimens, carefully designed to represent a wide range of geometries and loading conditions. The specimens were tested under multiaxial loading (including weld ends and continuous seam welds), and the FE models were built using the previously described shell meshing methodology implemented in NASTRAN. These elastic models captured the stress field around the weld toe accurately, even under multiaxial conditions, due to the stiffness fidelity ensured by the RBE2-based weld representation.

To link the simulation results with the experimental fatigue life, the Dang Van equivalent stress parameter τ_0 was used. This parameter accounts for both shear and hydrostatic stress, defined in the elastic regime by the relation:

$$\tau_o = \tau + \alpha * p \qquad \dots (4)$$

Where τ is the maximum shear stress over a load cycle, p is the hydrostatic pressure, and α is a material-dependent constant, found empirically.

For steels, Fayard's fatigue tests led to the determination of a reliable value of α =0.33, based on more than 200 fatigue tests conducted across various specimen types and materials. This value serves as a practical estimate, though ideally it should be calibrated through dedicated fully reversed bending and torsion tests to ensure maximum accuracy for a given material.

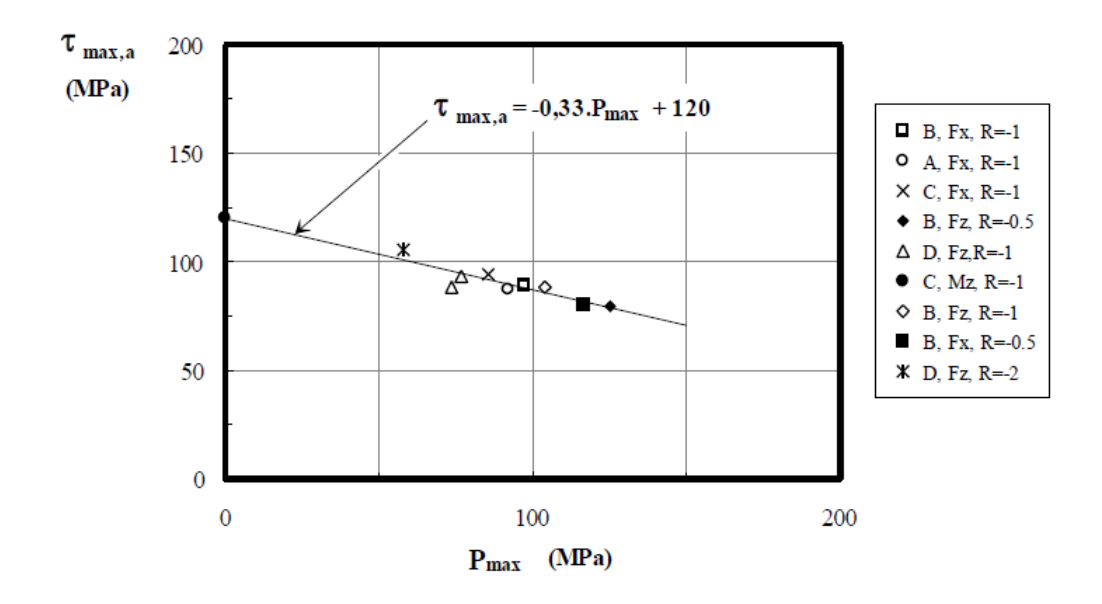


Figure 10. Mean fatigue strength at 10^6 cycles obtain from Fayard lab tests[1].

The fatigue failure criterion was defined not merely at crack initiation, but at the point where the crack grows beyond the local stress concentration zone—that is, when it exits the microstructural influence of the weld toe and enters a more stable propagation phase. Experimentally, this corresponds to a crack depth of approximately 0.5·e, where e is the sheet thickness, and a 30% drop in strain gauge signal at the hot spot location.

By applying the τ_0 stress parameter at the hot spot using the meshed shell model and correlating it to experimental fatigue life at 10^6 cycles, Fayard was able to produce a single τ_0 –N design curve. This curve is geometry- and load-independent, making it extremely valuable for industrial applications.

Tests

To validate the numerical fatigue methodology and assess the fatigue performance of welded joints, a series of controlled fatigue tests were performed on lap-jointed steel plates welded using Gas Metal Arc Welding (GMAW) with pulsed current (GMAW-P). The test specimens were fabricated from 2 mm-thick steel sheets with a yield strength of approximately 50 ksi. The geometry of the specimens, including weld dimensions and joint configuration, is shown in Figures X.

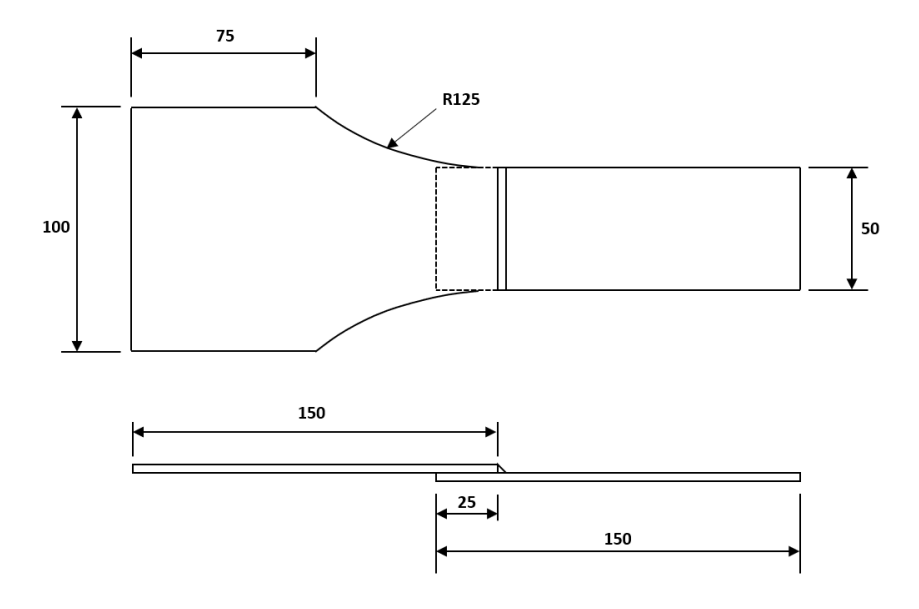


Figure 11. Dimensions for the Fx and Fy test probes

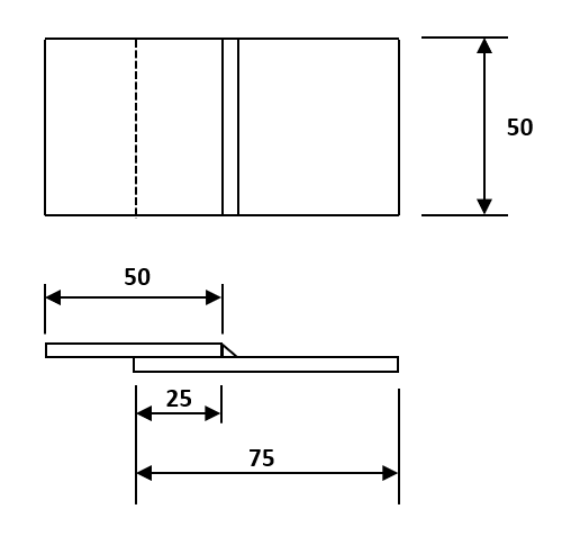


Figure 12. Dimensions for the four point bending (Fz) test

Welding Procedure and Parameters

The welding process was carried out using the following parameters:

Filler Metal: 0.035" ER70S-6

Shielding Gas: 90% Argon / 10% CO₂

Welding Mode: GMAW-P (Pulsed Gas Metal Arc Welding)

• Current: 130 A

Voltage: 21 V

Torch Angle: 60° relative to the surface
 Travel Speed: 25 inches per minute (ipm)
 Penetration: ~49% through thickness
 Weld Leg Length (average): 5 mm

This welding setup provided consistent quality across all specimens, ensuring controlled and repeatable fatigue results.

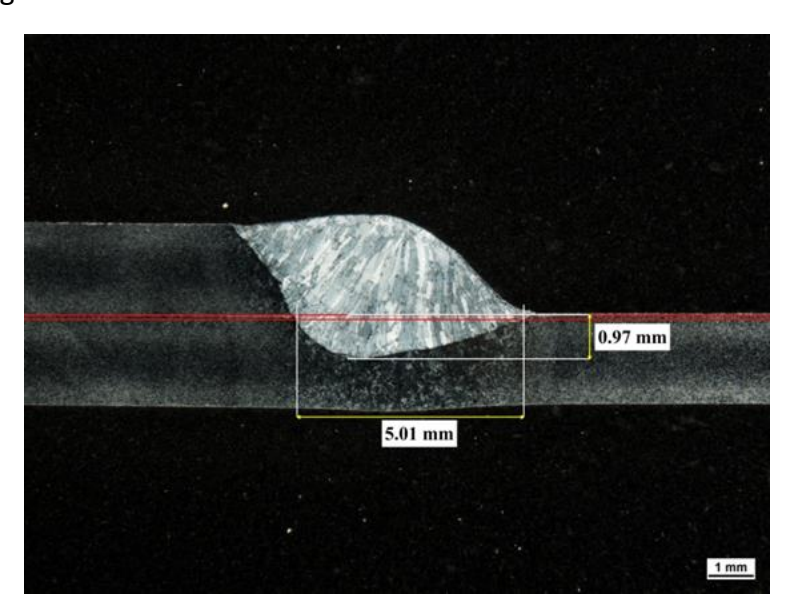


Figure 13. Lap weld lateral view

Loading Configurations

Fatigue testing was performed under three primary load cases, each designed to simulate different multiaxial stress states in the welded joint. All tests were conducted under constant amplitude cyclic loading with a load ratio R=0.1. The test conditions are summarized as follows:

Fx (Axial Loading):

- Load applied normal to the weld plane
- Load introduced at a distance of 75 mm from the weld centerline

Fy (Shear Loading):

Load applied parallel to the weld length, in-plane with the sheet

Applied at the same 75 mm offset

Introduces dominant shear stresses along the weld

Fz (Out-of-Plane Bending):

Performed a four-point bending test

Outer span: 90 mm

Inner span: 60 mm

Test Output and Data Handling

Each loading condition was tested across a range of force amplitudes, generating multiple data points for each load case. The output of each test was recorded as force amplitude versus number of cycles to failure (see Annex).

Calculations

To evaluate the applicability of the Fayard method in representing seam welds and analyzing their fatigue behavior using finite element modeling (FEM), experimental data from fatigue tests on welded joints were used. The specimens consisted of two steel plates of equal dimensions arranged in a lap joint configuration, joined by single-sided welds. Three different loading conditions were applied across the test series:

Axial Load (X-axis):

A uniaxial load was applied to the lower plate in the x-direction, introducing both normal (membrane) and bending stresses due to the eccentricity of the load relative to the weld plane. Consequently, the maximum stresses were concentrated near the root of the weld [24, 25].

19

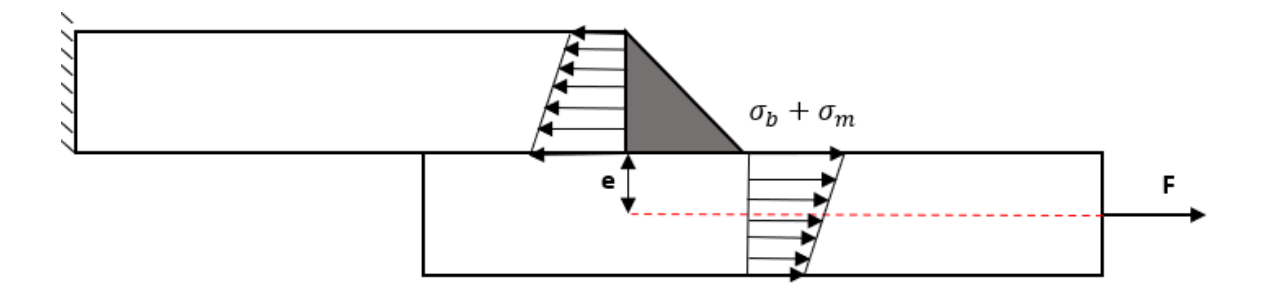


Figure 14. Stress Representation during the Fx Test

$$\sigma_m = \frac{F}{A} \qquad \dots (5) \qquad \qquad \sigma_b = \frac{6Fe}{bh^2} \qquad \dots (6)$$

Offset Load (Y-axis):

A load was applied in the y-direction, parallel to the weld seam and offset from the joint. This configuration primarily induced bending stress, leading to stress concentration near the weld on the loaded side.

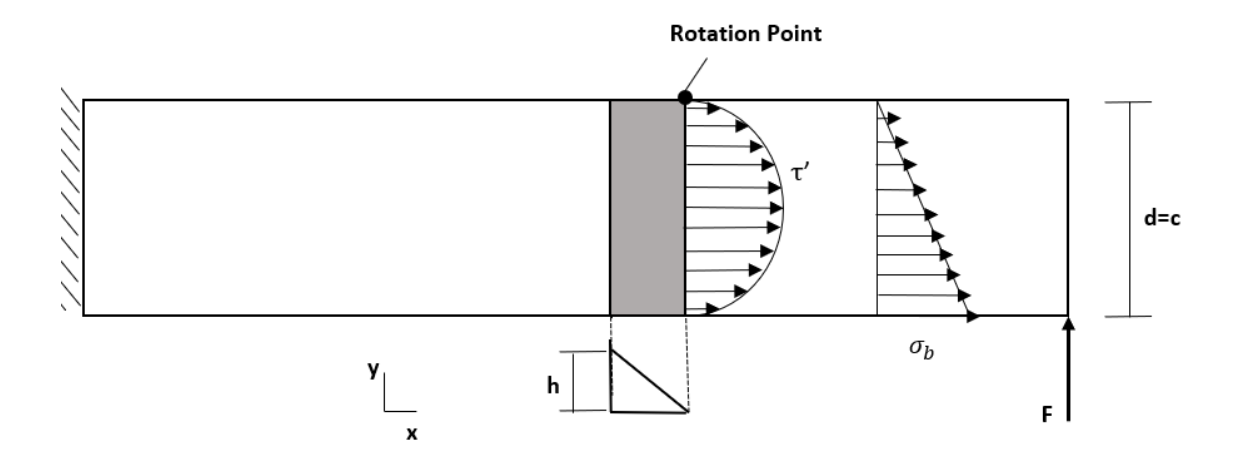


Figure 15. Stress Representation during the Fy Test

$$\tau' = \frac{F}{A} \qquad \dots(7) \qquad \sigma_b = \frac{Mc}{I} \qquad \dots(8)$$

$$I = 0.707h * I_u$$
 ... (9) $I_u = \frac{d^3}{12}$... (10)

Four-Point Bending (Z-axis):

The final test setup involved a four-point bending configuration, inducing bending stress along the z-axis. This arrangement ensured a region of pure bending between the inner supports, resulting in a uniformly distributed maximum stress across that region.

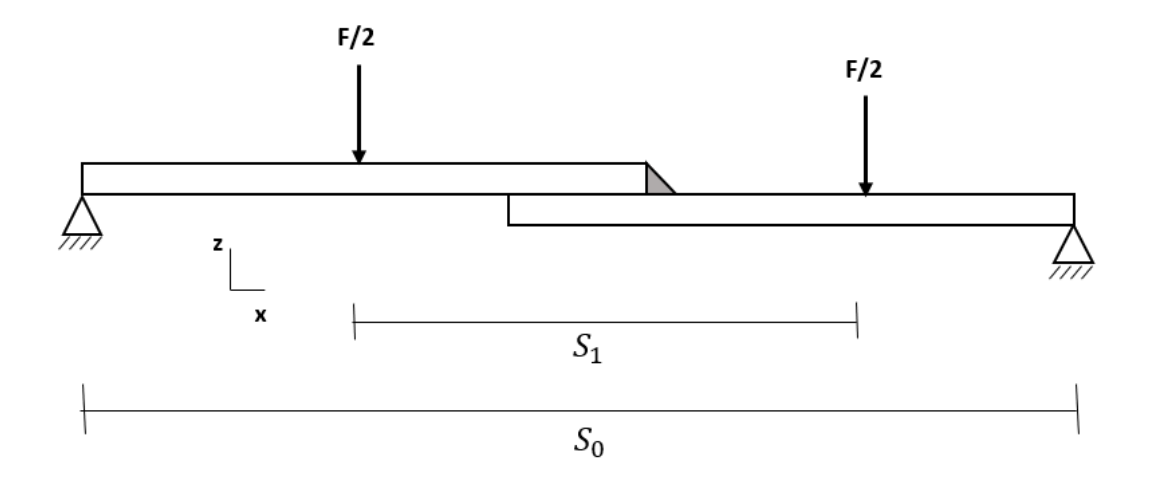
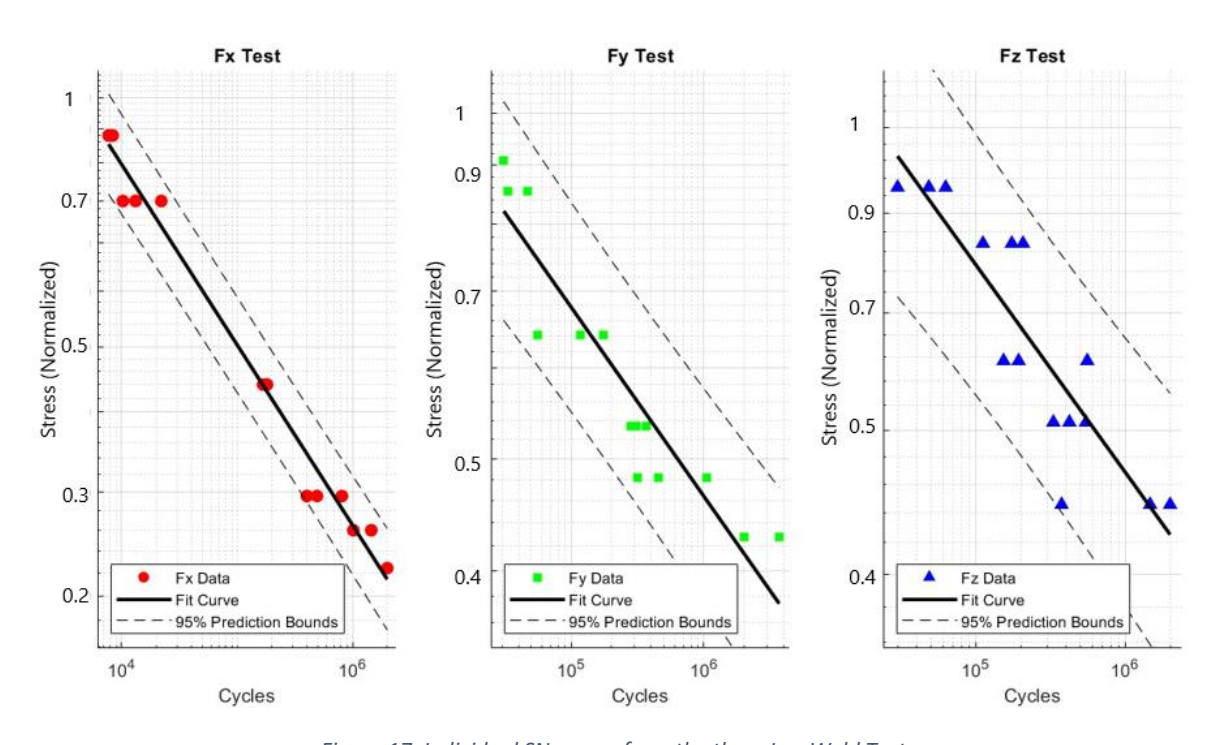


Figure 16. Load Representation during the Fz Test

$$\sigma = \frac{6M}{bh^2}$$
 ... (11) $M = F \frac{(S_o - S_1)}{4}$... (12)

Each test case was subjected to various load magnitudes to capture force (F) versus number of cycles to failure (N) data. As only force and fatigue life were directly measured, theoretical stress analysis was conducted to calculate the maximum stress for each configuration. Using these calculated stress values and the corresponding number of cycles to failure, S-N (stress-life) curves were constructed for each loading condition.

In addition to the mean S-N curves, 95% confidence intervals were determined. These intervals represent the range within which 95% of future test results are expected to fall, providing a statistical measure of the reliability and repeatability of the fatigue data. This is critical for engineering applications, as it helps to account for material variability and other uncertainties inherent in fatigue testing.



 ${\it Figure~17.~Individual~SN~curves~from~the~three~Lap~Weld~Tests.}$

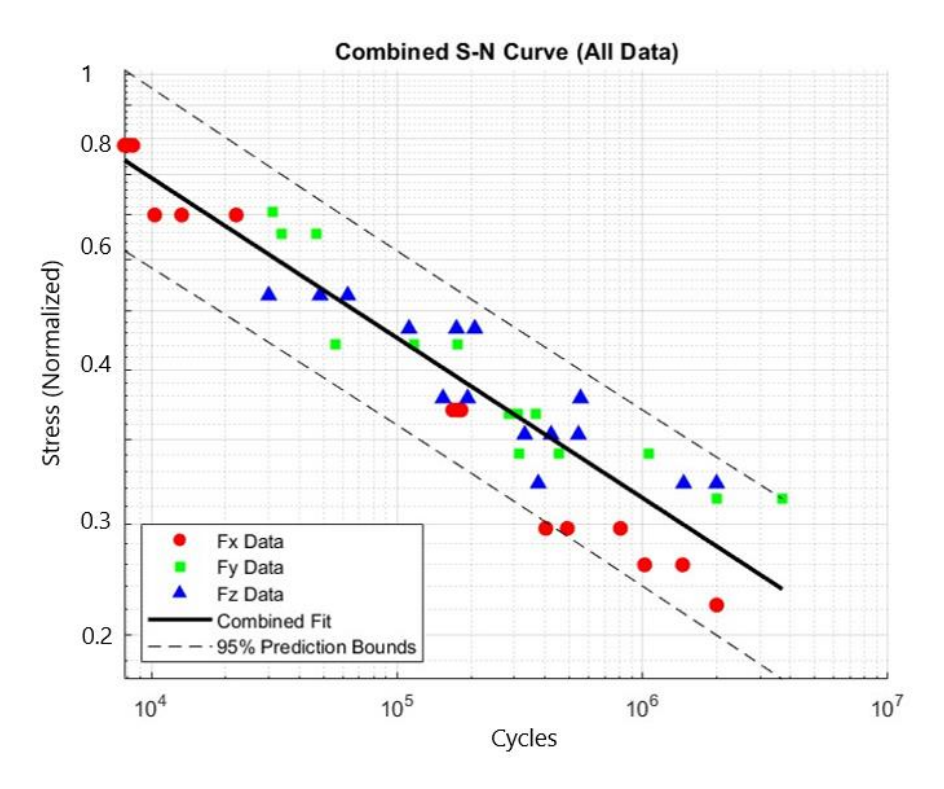


Figure 18. SN curved from the combined data of the Tests

The combined data resulted in an SN curve described by the following regression equation:

$$\sigma = A * N^B \qquad \dots (13)$$

where A and B are proprietary parameters calibrated through internal fatigue testing.

To illustrate the correlation between the theoretical stress calculations and the simulation results, three bar charts were prepared, each corresponding to one of the primary load cases (Fx, Fy, and Fz). In these plots, both the theoretical and simulated maximum principal stresses were normalized concerning the highest theoretical stress value observed across all cases. This normalization ensures that all results are expressed on a consistent, relative scale while protecting sensitive numerical data. The close alignment between the normalized theoretical and simulated stresses across all load cases demonstrates the accuracy and validity of the simulation model in reproducing the expected mechanical behavior. This supports the reliability of the finite element analysis methodology employed in this work.

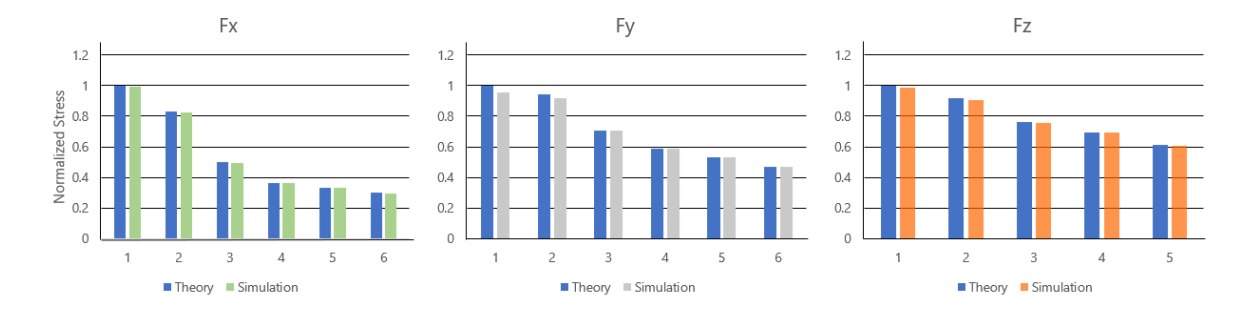


Figure 19. Comparison between the normalized stresses of theory and simulation

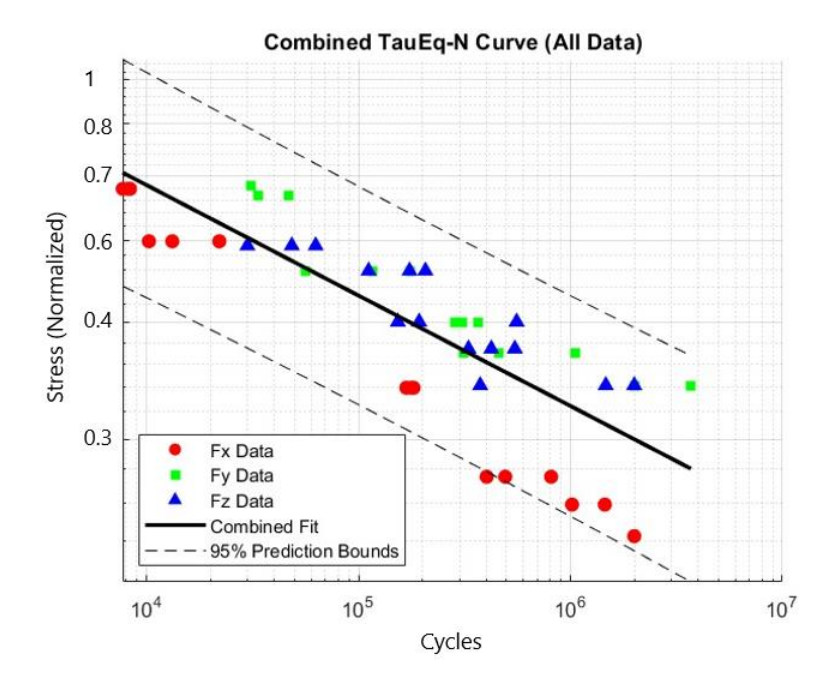


Figure 20. SN curve using Dang Van's Equivalent Stress

Just as with the SN curve using maximum principal stresses, the data of equivalent stress following Dang Van's Criterion resulted in the following regression equation:

$$\tau_{eq} = A * N^B \qquad \dots (14)$$

where A and B are proprietary parameters calibrated through internal fatigue testing.

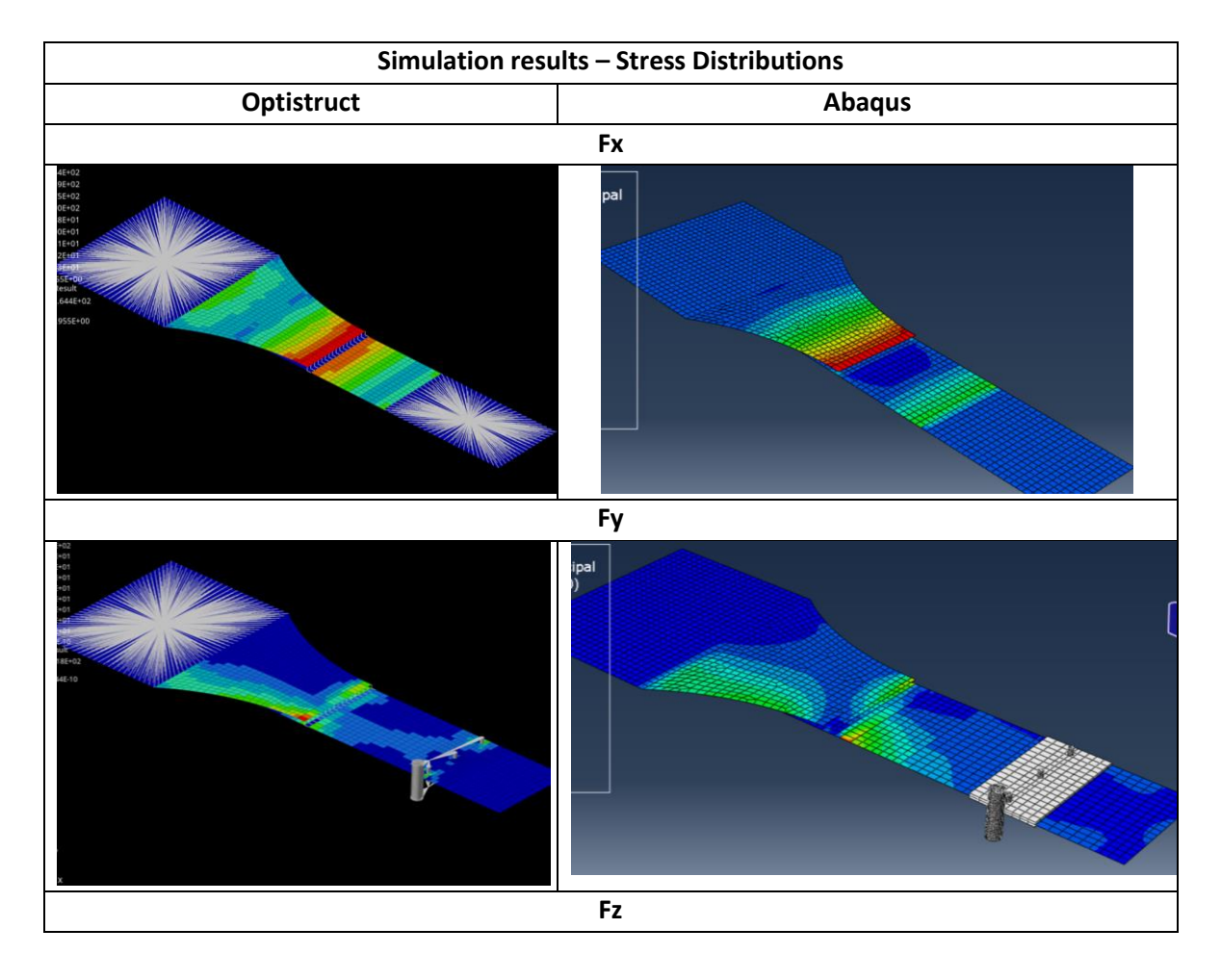
FEM analysis

Finite element models were developed using OptiStruct and Abaqus, following the specifications of the Fayard method, including weld dimensions and appropriate boundary conditions that replicated the experimental setups as closely as possible. For each test

scenario, the same load magnitudes applied in the experiments were imposed on the FEM models. The resulting maximum principal stresses from the simulations were extracted and compared to those calculated from theoretical models used in interpreting the experimental data.

The comparison between the simulated and theoretical maximum stresses showed good agreement, indicating that the Fayard method effectively captures both the load transmission and stress distribution characteristics in the weld region. Some discrepancies were observed, which can be attributed to factors such as:

- Residual stresses from the welding process,
- Variations in weld geometry and penetration,
- Microstructural inhomogeneities in the heat-affected zone (HAZ)
- Surface conditions and potential weld defects
- Misalignments or geometric tolerances in the test specimens
- Simplifications or assumptions made in the theoretical calculations (e.g., linear material behavior, perfect bonding).



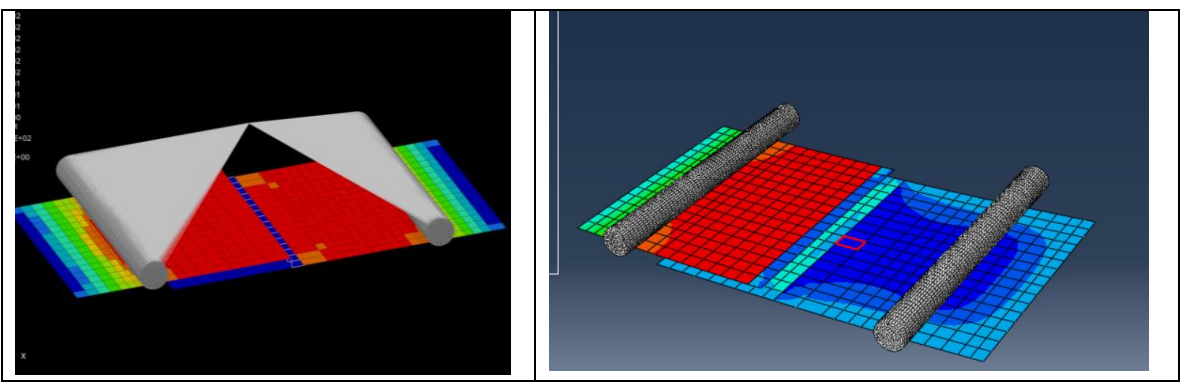


Table 1. Simulation results from Optistruct and Abagus

Validation with Different Joint Configurations

Additional experimental data were gathered using a different joint configuration to validate the applicability of the fatigue design curve obtained from the lap joint fatigue tests. In this case, T-joint welded specimens were tested, utilizing the same base material (2 mm thick 50 ksi steel) and the same welding procedure parameters as in the lap joint tests. This approach allows assessing whether the fatigue behavior characterized for one configuration can be reliably extrapolated to different structural geometries while maintaining similar welding conditions.

As with the lap joint specimens, fatigue tests were performed on the T-joint configurations, obtaining experimental force vs. number of cycles to failure data. These tests were carried out under controlled conditions, ensuring the same stress ratio (R = 0.1) for consistency with the earlier tests.

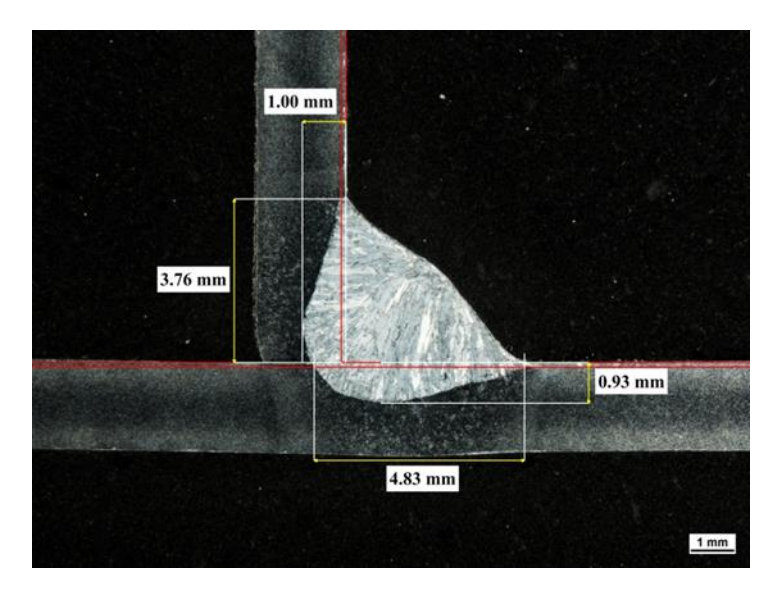


Figure 21. T-joint weld lateral view.

For the numerical analysis, finite element models of the T-joints were developed following the Fayard meshing methodology:

- Midsurfaces of the sheets were extracted to create shell models.
- Quadrilateral elements were used with refined mesh sizes near the weld toe, proportional to the weld leg length.
- The connection between plates and attachments was implemented using RBE2 rigid elements in OptiStruct and kinematic couplings in Abaqus, both providing accurate transmission of forces through the weld zone.
- The material was modeled with linear elastic properties, using the previously defined elastic modulus, Poisson's ratio, and density.

To validate the predictive capacity of the fatigue design curves obtained from the lap joint tests, additional tests were performed on welded T-joint specimens using the same material, welding process, and filler material. The data from these tests were compared with the prediction curves in two ways:

In the first approach, the fatigue life of each T-joint specimen was predicted by using the stress results obtained from the FEM simulations (maximum principal stress) as input into the SN curves derived from the lap joint tests. This provided direct fatigue life predictions that could be compared with the experimental results. The second approach involved plotting the experimental fatigue data of the T-joint specimens directly onto the SN and τ –N curves obtained from the lap joint experiments. This comparison allowed for a visual assessment of how closely the T-joint test results aligned with the fatigue behavior predicted by the lap joint-derived curves.

Overall, both approaches showed a good level of agreement between the simulations and the experimental data. Most of the data points fell within the prediction bounds for both the maximum principal stress-based SN curve and the equivalent stress-based τ –N curve. Notably, three outlier points were observed, all corresponding to tests from the Fz load case of the T-joint configuration. These points corresponded to the lowest applied load levels. They presented a particular challenge because they involved runout specimens that either failed at high numbers of cycles or did not fail at all during the test duration. This introduces some uncertainty and highlights the need for additional experimental testing in this specific loading condition to better define the fatigue behavior at lower stress ranges.

However, most of the experimental data aligned well with the fatigue predictions, supporting the robustness of the methodology based on the Fayard meshing rules and the SN/τ –N curves derived from the lap joint tests.

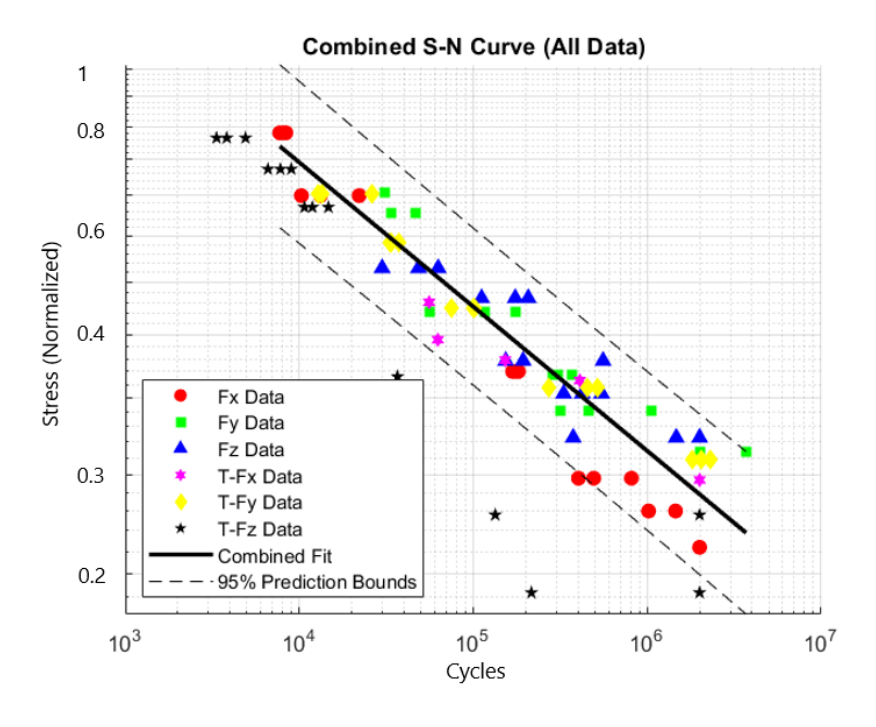


Figure 22. SN curve derived from lap weld tests and values of the T-Joint Tests

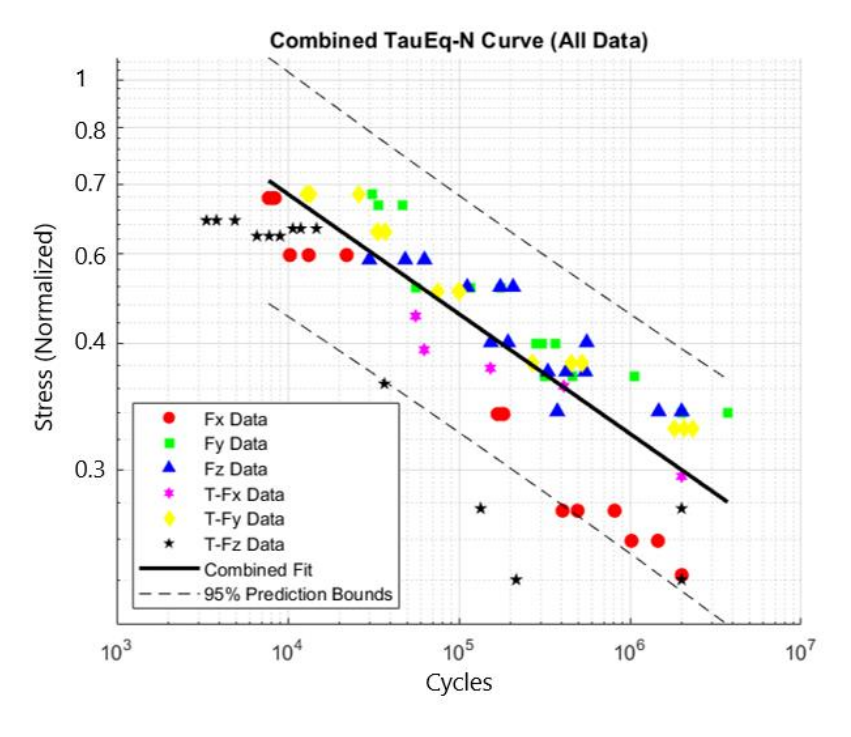


Figure 23. Tau-N curve derived from lap weld tests and values of the T-Joint Tests

SN Curve with Weibull Distribution

To complement the fatigue-life analysis previously conducted using a t-distribution—based regression model, a Weibull-based approach was also applied to obtain an alternative description of the experimental data. While the t-distribution model provides a reliable estimation of the mean S—N curve and its associated prediction bounds, it primarily reflects the uncertainty of the regression fit rather than the variability of the material's fatigue strength. Therefore, the Weibull model was implemented to describe the actual distribution of fatigue strength across specimens, enabling a deeper understanding of the material's reliability behavior.

The Weibull distribution is widely recognized in fatigue and reliability analysis due to its versatility in modeling life- and strength-related random variables [26, 27]. For a given number of cycles to failure N, the probability density function (PDF) of the stress amplitude S is expressed as:

$$f(S \mid \eta, k) = \frac{k}{\eta} \left(\frac{S}{\eta}\right)^{k-1} exp\left[-\left(\frac{S}{\eta}\right)^{k}\right] \qquad \dots (15)$$

where:

k is the shape parameter, which defines the degree of scatter (higher k values indicate lower variability), and η is the scale parameter, corresponding approximately to the stress level at which 63.2% of specimens are expected to fail.

To link the distribution parameters to fatigue life, the scale parameter was modeled as a function of the number of cycles using a log-linear relation:

$$\eta(N) = e^{a+blnN} \qquad \dots (16)$$

Where a and b are material constants that define how fatigue strength decreases with increasing life. This expression is equivalent to the Basquin equation, $\sigma=A*N^B$, where $\sigma=e^a$ and m=b but formulated within the Weibull context.

The parameters a, b, and k were estimated using the Maximum Likelihood Estimation (MLE) method, which determines the parameter set that maximizes the probability of observing the experimental data given the assumed model [27]. For a dataset of stress–life pairs (S_i, N_i) , the likelihood function is taken as :

$$\ln L(a,b,k) = \sum_{i=1}^{n} \left[\ln k - \ln \eta(N_i) + (k-1) \ln \left(\frac{S_i}{\eta(N_i)} \right) - \left(\frac{S_i}{\eta(N_i)} \right)^k \right] \dots (17)$$

The parameters were obtained by maximizing $\ln L$, or equivalently, by minimizing the negative log-likelihood using MATLAB's fminunc solver. The resulting optimal values a', b', and k' define the best-fit Weibull model representing the observed fatigue data.

Once the Weibull parameters were determined, quantile S–N curves were generated to represent different probabilities of failure. The obtained curves where:

- $S_{0.50}(N)$: median or 50% failure probability (expected behavior),
- $S_{0.05}(N)$: 5% quantile (95% survival probability, conservative design curve),
- $S_{0.95}(N)$: 95% quantile (upper scatter limit)

Plotting these quantile curves together with the experimental data provides a visual representation of the distribution of fatigue strengths and their probabilistic boundaries as seen in Figure 24 where the Tau-N curve was derived.

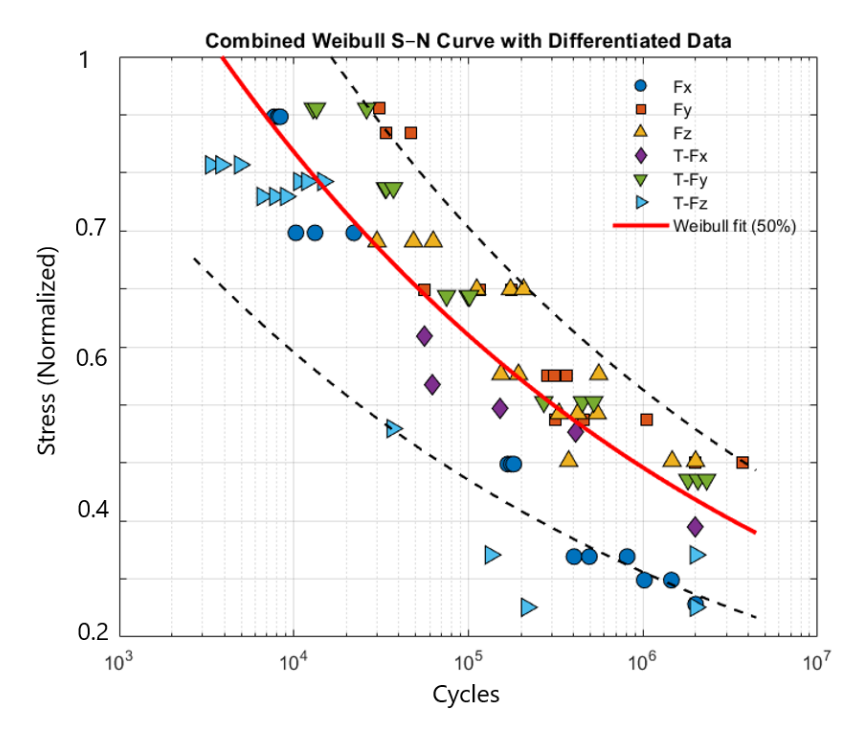


Figure 24. Weibull Tau-N curve derived from lap weld tests and values of the T-Joint Tests

The Weibull-based S–N curve differs conceptually from the t-distribution regression approach. In the t-distribution model, the 95% prediction bounds quantify the uncertainty in the estimated mean curve, reflecting how confidently the regression predicts new data. In contrast, the Weibull quantile curves directly represent the probability of failure for the population of specimens, thereby describing the inherent variability of the material itself.

This makes the Weibull model particularly valuable for reliability-based design, where engineers must determine allowable stress levels corresponding to specified survival probabilities.

Simulation Procedure for OptiStruct and Abaqus

A detailed, step-by-step simulation procedure, which is outlined in the annexes, has been developed for both Altair OptiStruct and Abaqus to facilitate the practical application of the methodology presented in this work. These procedures serve as useful guides for engineers and researchers aiming to implement fatigue analysis of welded joints using the approach described throughout this thesis. The guidelines encompass the entire modeling process, from meshing according to Fayard's methodology to assigning material properties, boundary conditions, and loading.

For such guidelines, the element size in the vicinity of the weld was selected to be proportional to the weld leg dimensions to ensure an accurate representation of stress gradients. Ideally, this mesh refinement would be defined during CAD preprocessing to precisely delimit the weld region; however, if such preprocessing is not feasible, the mesh density must be manually adjusted to approximate the weld dimensions as closely as possible. Quadrilateral elements were used in all critical regions to improve accuracy. The weld itself was modeled with rigid connections, utilizing RBE2 elements in OptiStruct or Kinematic Couplings in Abaqus, which provided a realistic approximation of the stiffness introduced by the seam weld. Once solved, this model allowed for straightforward extraction of the maximum principal stress or the combination of maximum shear stress and hydrostatic pressure required to compute the equivalent stress according to the Dang Van criterion. These stresses were then related to the material fatigue properties through the SN curve to estimate the number of cycles to failure for each loading condition. By following these structured steps, users can perform reliable fatigue assessments without requiring specialized fatigue software, while still achieving meaningful predictive results for welded structures.

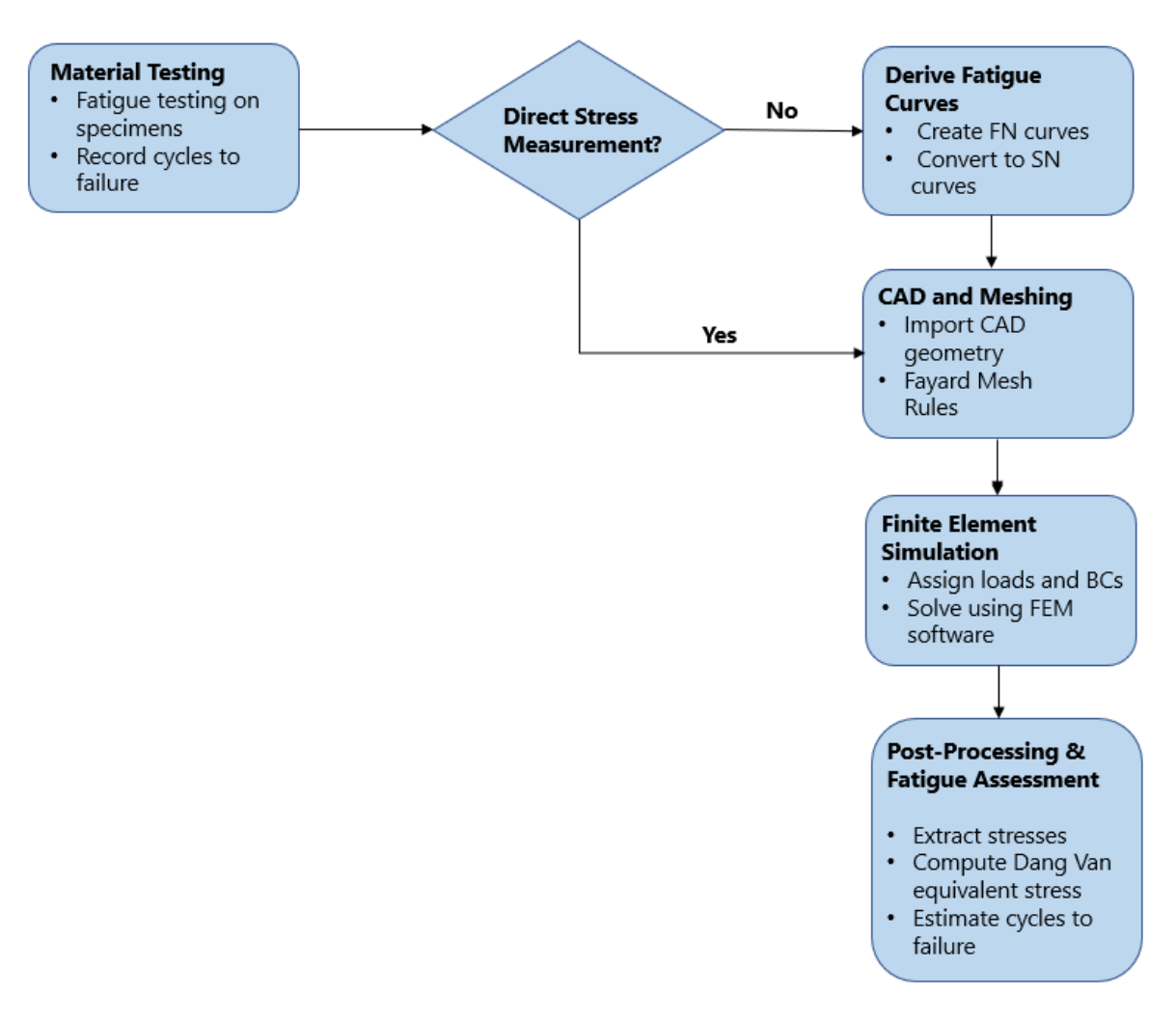


Figure 25. Overall workflow of the methodology

Process automation:

While the manual implementation of Fayard's methodology provides a valuable understanding of the meshing rules and load transfer representation, its application to larger or more complex welded structures can quickly become time-consuming and prone to modeling inconsistencies. To overcome this limitation, a custom plugin for Abaqus was developed as part of this thesis.

The plugin was created using Python scripting and the Abaqus RSG Builder framework, which enabled the direct integration of a graphical user interface (GUI) into Abaqus/CAE (Figure 19). The tool automates the construction of the seam weld model by generating the weld mesh and rigid connections according to Fayard's meshing rules.

The inputs required by the plugin are:

- Weld leg size: used to define the dimensions of the first mesh elements adjacent to the weld and the position of the rigid elements.
- Selection of three reference edges in the CAD geometry: these must be present in the 3D model and are used to define the weld location and orientation in the assembly.

Once these inputs are provided, the plugin automatically builds the mesh for the welded connection and inserts the rigid coupling elements that simulate load transfer between the plates, ensuring consistency with Fayard's methodology. This eliminates the need for manual construction of each rigid link, which is one of the most tedious aspects of the process.

In addition to the modeling tool, a post-processing plugin was developed (Figure 20). This tool extracts stress data from the analysis results, computes the equivalent stress parameter (τ _eq) based on Fayard's adaptation of the Dang Van criterion, and estimates the number of cycles to failure under the applied loading conditions. This functionality provides a direct link between FEM results and fatigue assessment without requiring specialized fatigue analysis software such as Fe-Safe or nCode.

Together, these tools enable the transition from manual validation of Fayard's methodology to a practical workflow for industrial applications, ensuring that engineers can apply the method efficiently to real-world components.

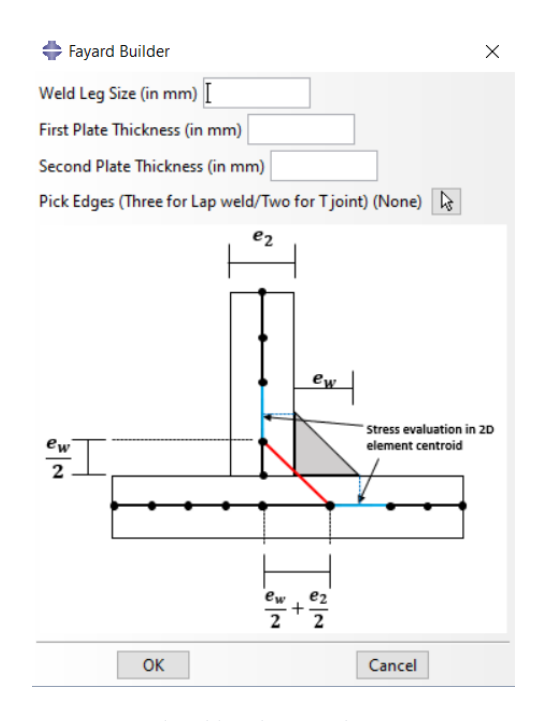


Figure 26. Fayard Builder Plugin with its two main inputs.

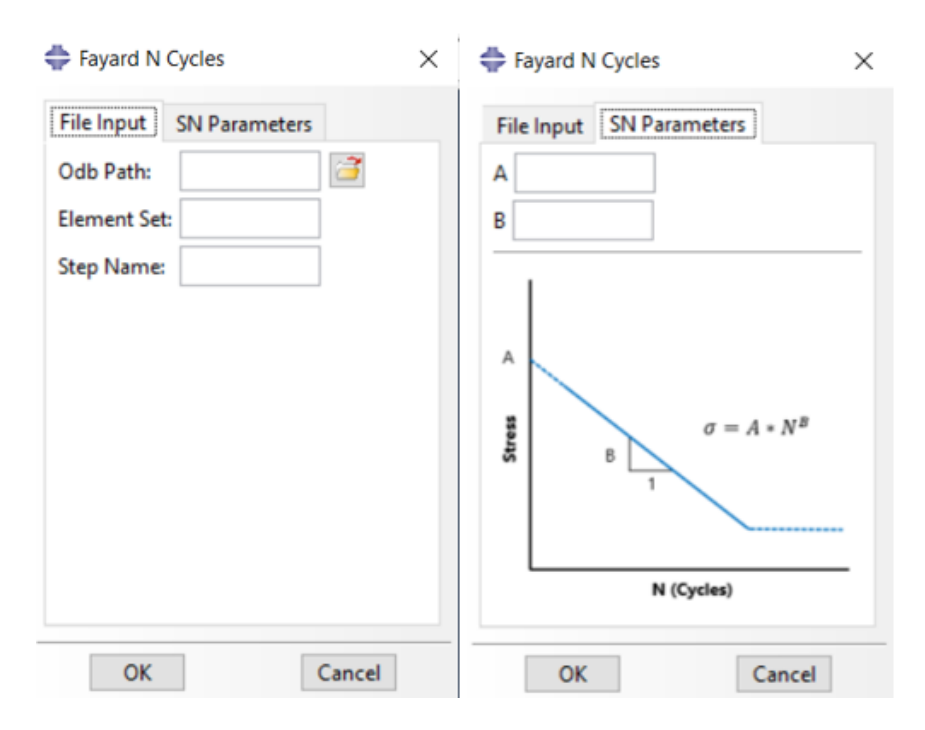


Figure 27. Fayard Post processing plugin.

Conclusion

The present study focused on the fatigue analysis of welded thin-sheet steel structures using the meshing methodology developed by Fayard et al. and applying fatigue assessment approaches such as the structural hot-spot stress method and the Dang Van multiaxial fatigue criterion. The methodology was validated through experimental testing and finite element simulations, and its applicability for automotive thin-sheet weld structures was evaluated.

Main Findings:

Correlation between Simulations and Experiments:

The comparison between the experimental results and the fatigue life predictions from the FEM simulations revealed a good correlation when using the maximum principal stress as the fatigue-driving parameter, especially at the weld toe where fatigue cracks typically initiate. This indicates that, for welded thin-sheet structures under similar conditions, the use of maximum principal stress provides a reliable estimate of fatigue life.

Performance of the Equivalent Stress (τ_0):

Slightly larger deviations were observed when using the equivalent stress parameter (τ_0) derived from Fayard's adaptation of the Dang Van criterion. This is likely since the slope (0.33) used in the calculation of τ_0 comes from Fayard's original tests, which were performed on different geometries and loading configurations.

To improve accuracy, future studies should aim to replicate Fayard's experimental procedure, including full bending and full torsion tests, to derive a τ_0 -N curve specifically adapted to the materials and welding configurations employed in this work.

Recommendations for Improved Correlation:

Additionally, installing strain gauges near the critical welding zones during testing could provide direct stress measurements to compare with FEM results. For optimal placement

of these strain gauges, preliminary FEM simulations are recommended to identify the locations of maximum expected stresses.

Validation of Fayard's Methodology:

Despite the deviations mentioned above, this study confirms that Fayard's meshing rules and methodology provide a robust framework for evaluating the fatigue behavior of welded thin-sheet structures. The implementation in both OptiStruct and Abaqus was straightforward, with rigid connections (RBE2 elements or kinematic couplings) enabling proper stress transfer between welded components.

Practical Implementation:

A detailed step-by-step guide for applying this methodology in both OptiStruct and Abaqus was developed, enabling engineers to use it in the design process. Furthermore, the model's simplicity and efficiency mean that specialized fatigue analysis software (e.g., nCode, Fe-Safe) is not required, although such tools could provide access to additional fatigue analysis parameters and visualization features if needed.

Automation through Plugin Development:

Recognizing the repetitive and error-prone nature of manual modeling following Fayard's rules, two Abaqus plugins were developed as part of this work:

Modeling plugin – Created with Python and the Abaqus RSG Builder, this tool automates the meshing of welded joints and the generation of rigid elements that represent weld load transfer. Inputs include the weld leg size and the selection of three reference edges on the CAD model to define the weld location. This significantly reduces modeling time and improves consistency across different studies.

Post-processing plugin – This tool extracts FEM stress results and computes both the equivalent stress parameter (τ_eq) and the corresponding fatigue life (N) based on the

obtained SN curves. It provides engineers with a direct bridge between FEM results and fatigue assessment, without requiring third-party fatigue software.

Together, these plugins transform Fayard's methodology into a practical and efficient workflow, enabling faster modeling, automated data treatment, and reproducible fatigue assessments for thin-sheet welded structures.

Final Remarks:

This research demonstrates that a reliable fatigue analysis of thin-sheet welded structures can be performed using standard FEM software combined with Fayard's meshing strategy and suitable fatigue criteria. While refinements in test procedures and local measurement strategies could further improve predictive accuracy, the foundation laid by this work is sufficient to support the practical design of welded thin-sheet components subjected to fatigue loading.

Further work:

Future work should include the replication of Fayard's full experimental procedure (bending and torsion tests) to obtain parameters directly applicable to the studied material and joint configurations. Furthermore, the developed plugins can be extended by integrating automatic SN curve fitting, improved visualization of fatigue-critical regions, and compatibility with additional solver environments. This evolution would further strengthen the practicality and versatility of the methodology, opening the path for broader industrial adoption of seam weld fatigue assessment.

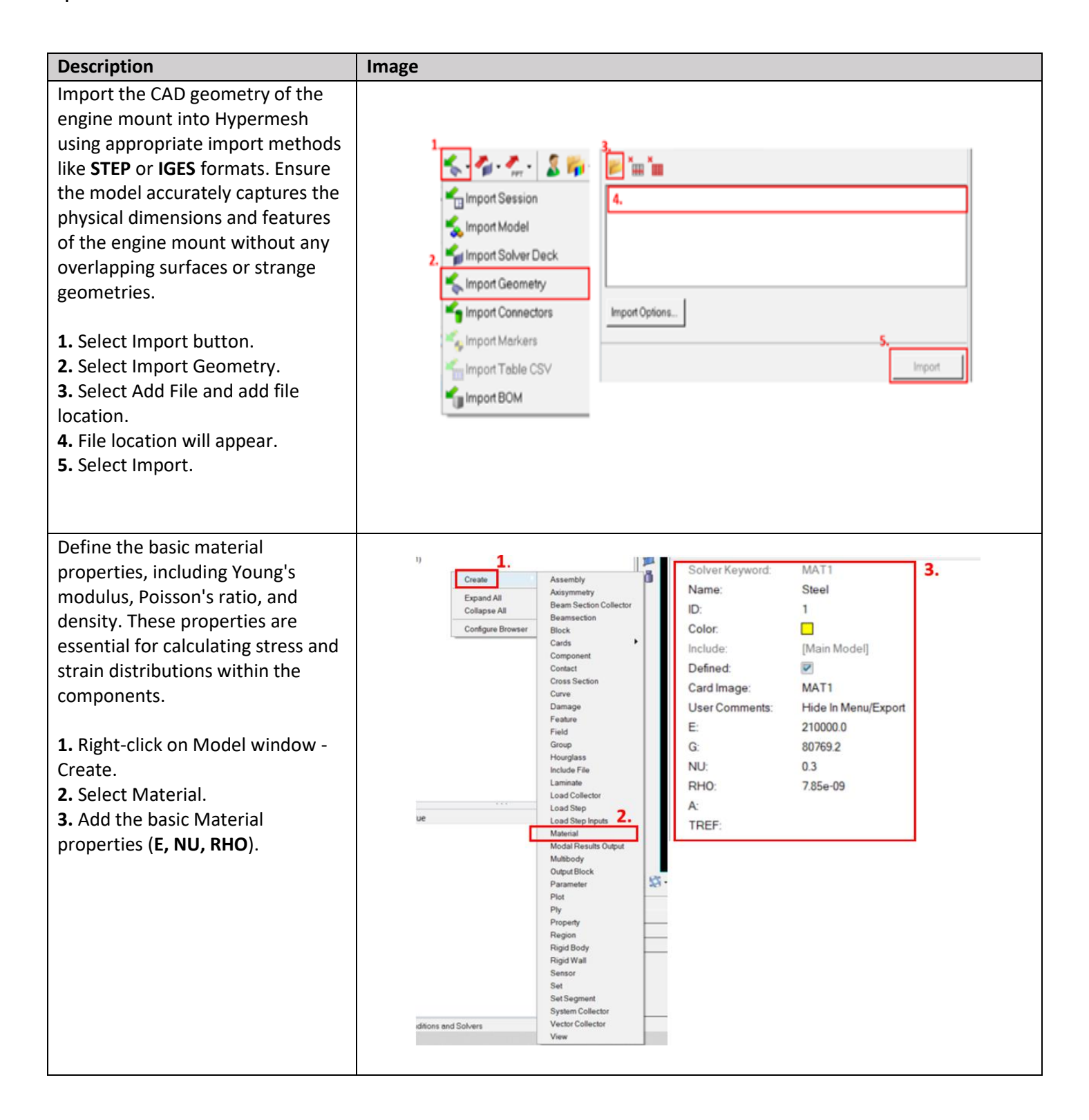
References

- [1] J.L. Fayard, "Dimensionnement à la fatigue polycyclique de structures soudées," Thèse, École Polytechnique, 1996.
- [2] K. Dang Van, A. Bignonnet, J.L. Fayard, "Assessment of welded structures by a structural multiaxial fatigue approach," Biaxial/Multiaxial Fatigue and Fracture, Elsevier Science Ltd. and ESIS, Publication 31, 2003.
- [3] W. Fricke, "IIW guideline for the assessment of weld root fatigue," Weld World, vol. 57, no. 6, pp. 753–791, 2013. doi:10.1007/s40194-013-0066-y.
- [4] D. Turlier, P. Klein, F. Bérard, "Seam Sim method for seam weld structural assessment within a structure FEA," Proc. Int. Conf. AWST 2010, GEDIK Education Foundation, Istanbul, pp. 651–658, 2010.
- [5] D. Turlier, P. Klein, F. Bérard, "FEA shell element model for enhanced structural stress analysis of seam welds," Weld World, vol. 58, pp. 511, 2014. doi:10.1007/s40194-014-0134-y.
- [6] D. Devarasiddappa, "Automotive Applications of Welding Technology A Study," International Journal of Modern Engineering Research (IJMER), vol. 4, no. 9, pp. 13–19, 2014.
- [7] M. Kimchi and D. H. Phillips, Resistance Spot Welding: Fundamentals and Applications for the Automotive Industry. Morgan & Claypool Publishers, 2017.
- [8] "What is Spot Welding? (A Complete Welding Process Guide)," The Welding Institute. [Online]. Available: https://www.twi-global.com/technical-knowledge/faqs/what-is-spot-welding
- [9] K. Weman, "Pressure welding methods," in Welding Processes Handbook, 2nd ed., K. Weman, Ed., Woodhead Publishing, pp. 119–132, 2012.
- [10] "What is Resistance Welding? Process, Diagram, Types & Applications," Electrical Workbook. [Online]. Available: https://electricalworkbook.com/resistance-welding/
- [11] S. T. Riches, "Industrial lasers and applications in automotive welding," presented at the Make It With Lasers™ Workshop: Lasers in the Automotive Industry, Nissan Motor Manufacturing (UK) Ltd., Sunderland, U.K., Oct. 22, 1998. [Online]. Available: https://www.twi-global.com/technical-knowledge/published-papers/industrial-lasers-and-applications-in-automotive-welding/
- [12] Olabi, A.G., "Comprehensive Materials Processing, Review of Microstructures, Mechanical Properties, and Residual Stresses of Ferritic and Martensitic Stainless-Steel Welded Joints", pp 181–192, 2014.
- [13] "What is Laser Beam Welding? Complete Explanation," The Welding Master. [Online]. Available: https://theweldingmaster.com/laser-beam-welding/
- [14] "MIG vs TIG welding (What is the difference between them?)," TWI Ltd., [Online]. Available: https://www.twi-global.com/technical-knowledge/faqs/mig-vs-tig-welding#MIGProcess

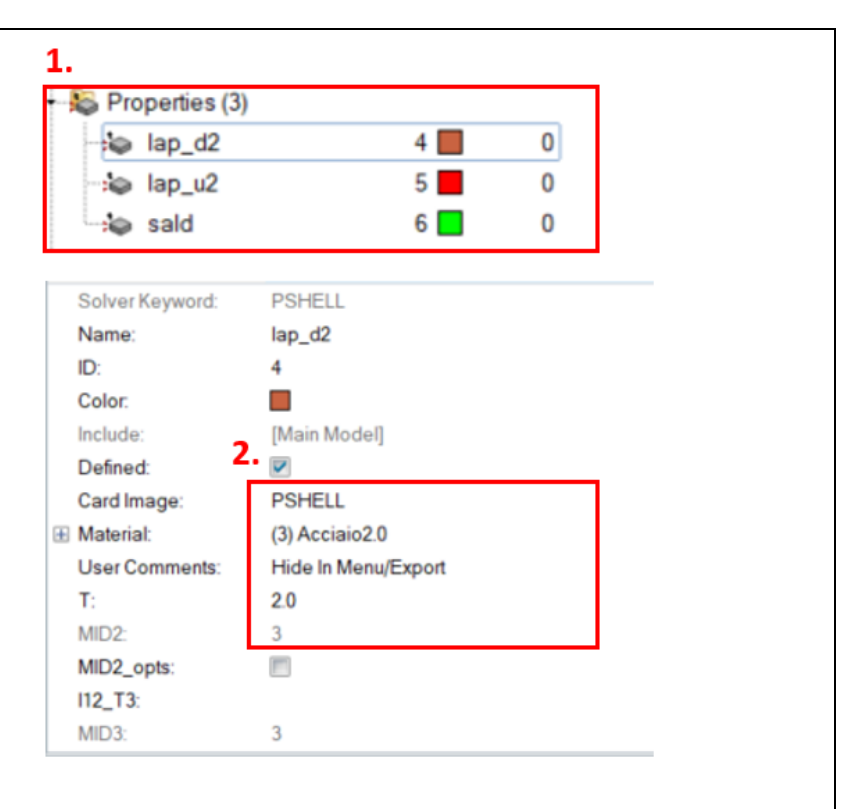
- [15] "MIG vs TIG Welding Main Differences Explained," Fractory, [Online]. Available: https://fractory.com/mig-vs-tig-welding/
- [16] "What is Friction Stir Welding (FSW)? Process and Applications", TWI Ltd., [Online]. Available: https://www.twi-global.com/technical-knowledge/faqs/faq-what-is-friction-stir-welding
- [17] "Friction stir welding of aluminium alloys," TWI Ltd., [Online]. Available: https://www.twi-global.com/technical-knowledge/published-papers/friction-stir-welding-of-aluminium-alloys
- [18] D. Radenkovic, Stress analysis in tubular joints. Proceedings of the international conference, Steel in marine structures, Doc. EUR 7347. Pub. IRSID St Germain en Laye, pp. 71-1 18, 1981.
- [19] Z. Barsoum, Guidelines for Fatigue and Static Analysis of Welded and Un-welded Steel Structures, KTH Royal Institute of Technology, Stockholm, Sweden, 2020.
- [20] K. Dang Van, Sur la résistance à la fatigue des métaux, Sciences et Techniques de l'Armement, vol. 47, no. 5, pp. 479–495, 1973.
- [21] Bignonnet, A., Fatigue Design in Automotive Industry, in High Cycle Metal Fatigue: From Theory to Applications, C.I.S.M. Courses and Lectures No. 392, Eds. Ky Dang Van & Ioannis V. Papadopoulos, Springer, 1999, pp. 145–168.
- [22] Jean-Luc Fayard, André Bignonnet, Ky Dang Van. Fatigue design criterion for welded structures. Fatigue and Fracture of Engineering Materials and Structures, 1996.
- [23] Fayard, J.-L., Bignonnet, A., Dang Van, K., Fatigue Design of Welded Thin Sheet Structures, In Proc. Fatigue Design '95, Eds. Marquis, G. and Solin, J., Helsinki, Finland, 5–8 Sept. 1995
- [24] R. G. Budynas and J. K. Nisbett, Shigley's Mechanical Engineering Design, 9th ed. New York, NY, USA: McGraw-Hill, 2011.
- [25] "Eccentric Bending Moment Single Side Fillet Welds," SolidWorks Help, SolidWorks Corporation. [Online]. Available:
- https://help.solidworks.com/2020/english/SolidWorks/cworks/c Eccentric Bending Moment SS Welds.htm.
- [26] Weibull, W. "A Statistical Distribution Function of Wide Applicability. Journal of Applied Mechanics", 18(3), pp 293–297. 1951.
- [27] Castillo, E., & Fernández-Canteli, A. (2009). A Unified Statistical Methodology for Modeling Fatigue Damage. Springer.
- [28] "Efficient FE Modelling Course: Scripting Abaqus CAE using Python," Martin Pletz. [Online]. Available:
- https://www.researchgate.net/publication/345680663 Efficient FE Modelling Course Scripting Abaqus CAE using Python
- [29] P. Gautam. "Python Scripts for Abaqus: Learn by Example," 2011.

Annexes

Optistruct



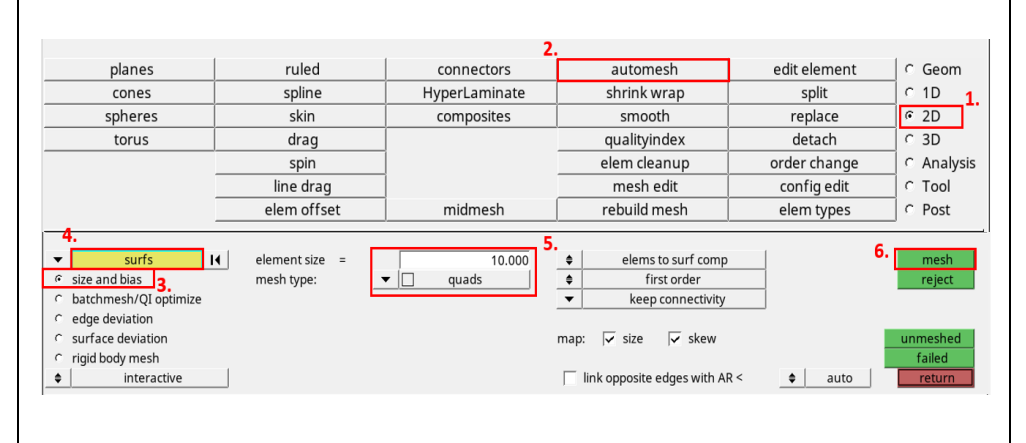
Define the properties of the components, which in this case must be defined as shells.1. Right-click on Model window - Create.2. Add the Card Image **PSHELL**, select the material defined previously, and the **surface thickness**.

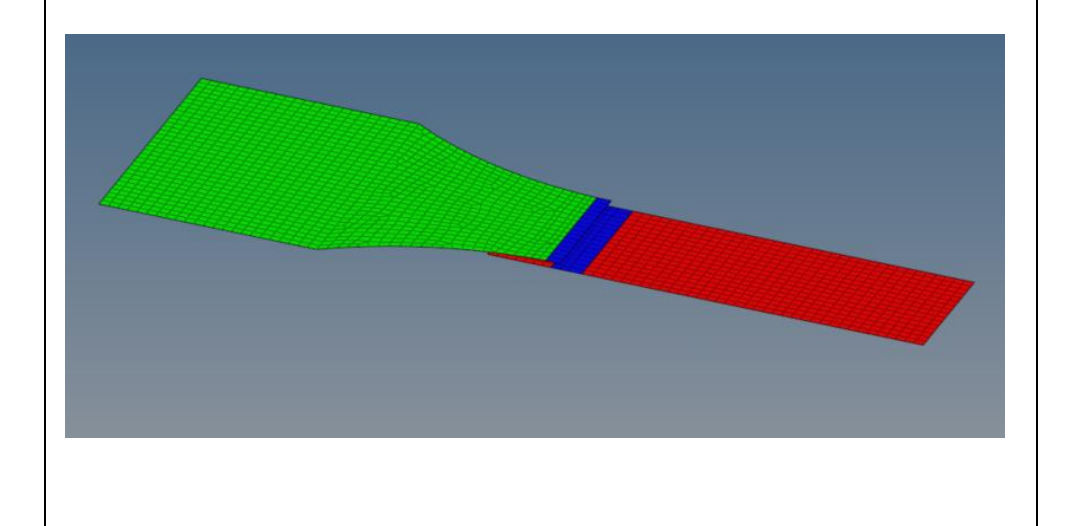


Generate the mesh following the meshing rules established by Fayard. The mesh size must be based on the weld leg length.

If possible make sure to create a component of the areas near the weld, to facilitate mesh size and to identify quickly the stresses during postprocessing:

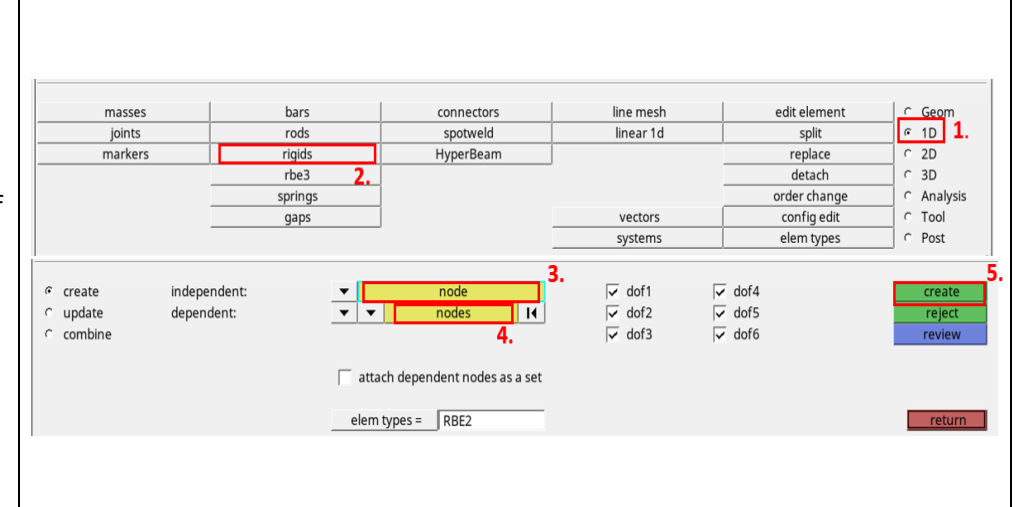
- 1. Select 2D options.
- 2. Select Automesh.
- 3. Select Size and Bias.
- 4. Select the surfs to mesh.
- **5.** Select source type QUAD and input the element size.
- 6. Mesh.

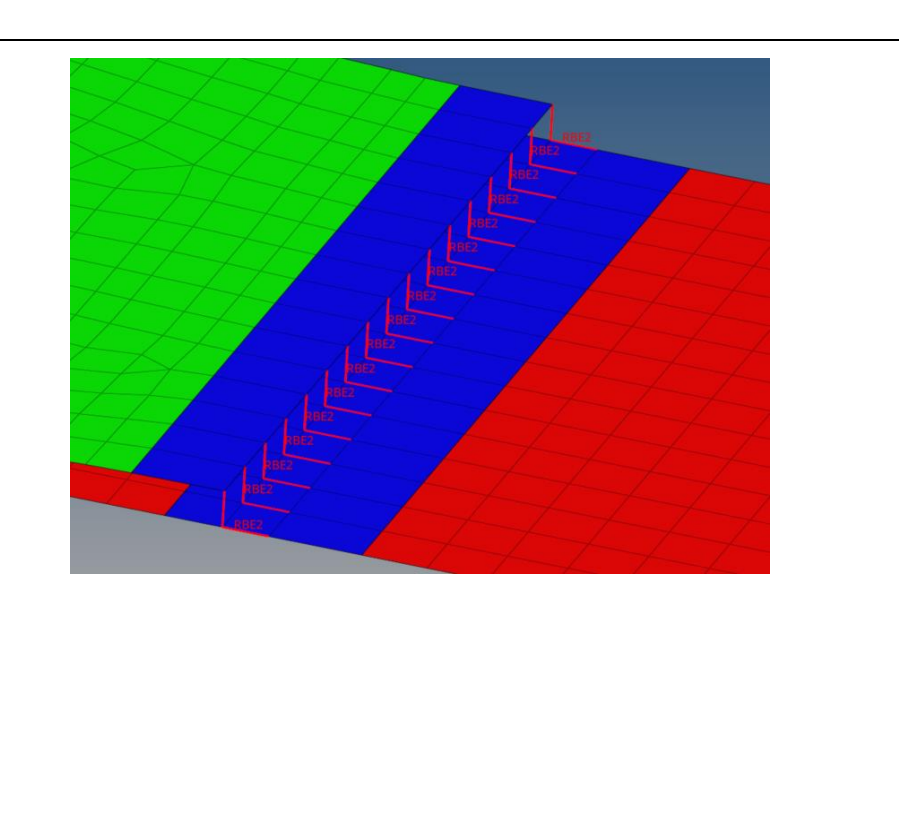




To create the weld representation, rigid elements type **RBE2** are the most appropriate choice since they give the necessary rigidity that is formed by the weld. Such elements allow the transmission of stresses through the components.

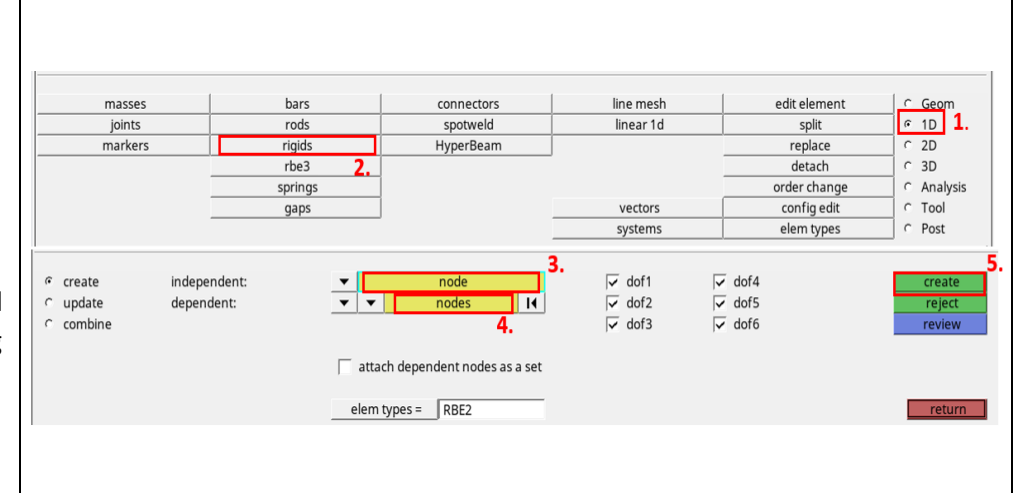
- 1. Select 1D options.
- **2.** Select Rigid elements.
- **3.** Select the independent node.
- **4.** Select the dependent node to connect both parts.
- **5.** Select Create.
- **6.** Repeat until the nodes between both sections are connected.

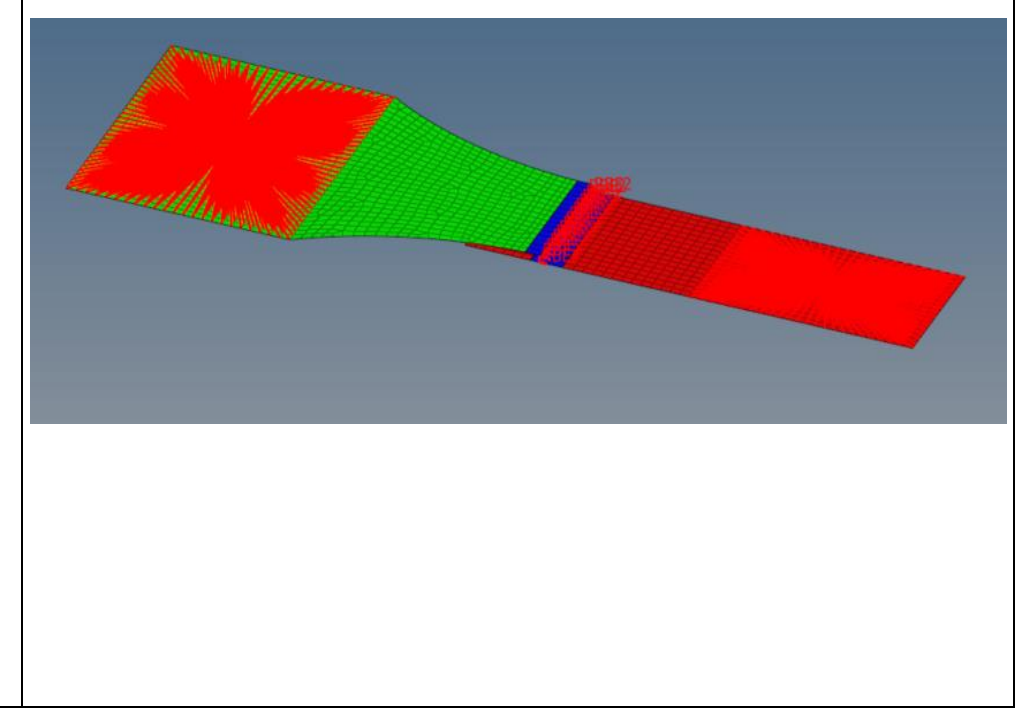


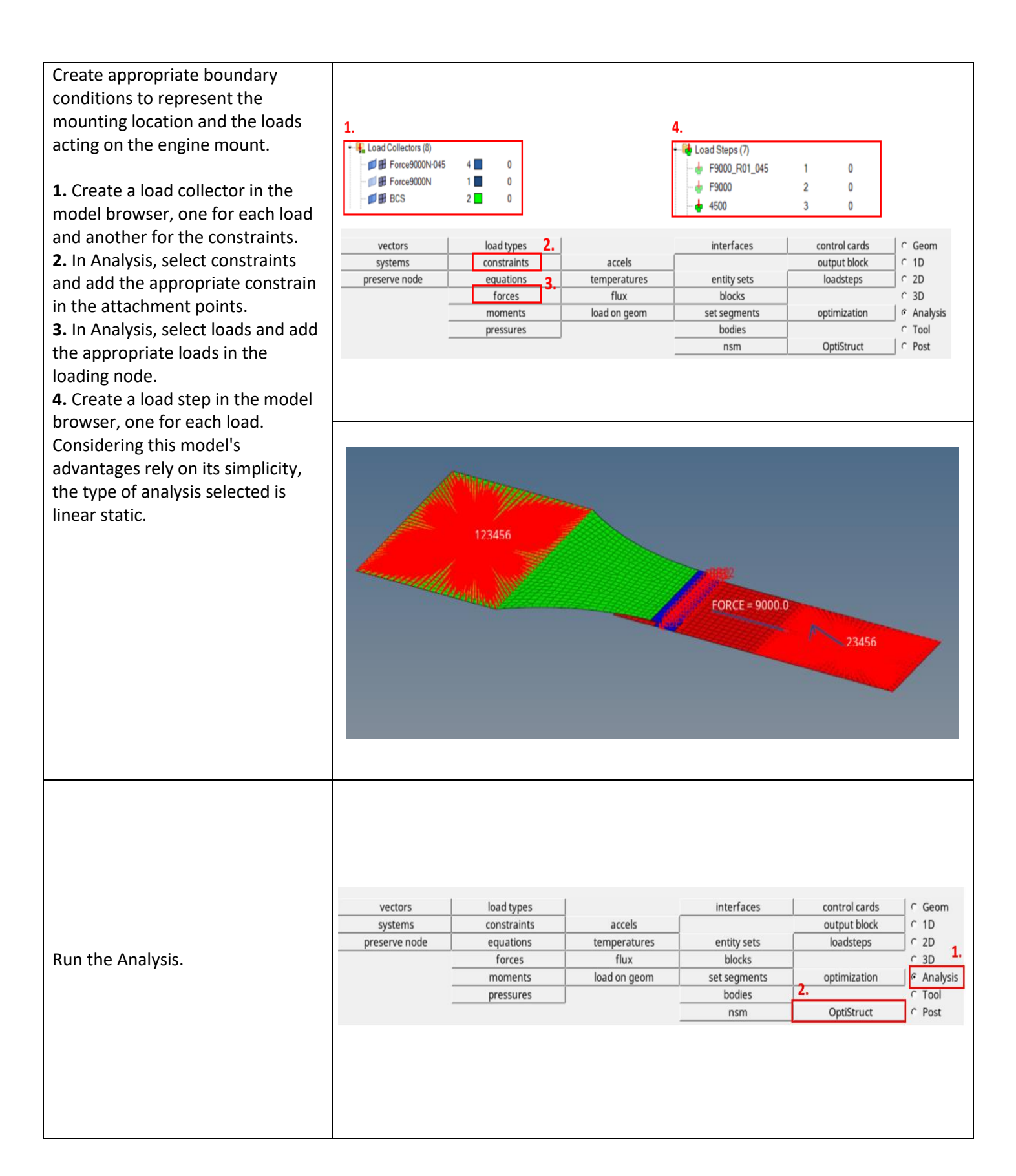


Create appropriate boundary conditions to represent the fixing conditions and the loads acting on the component. In this example, using one of the lap weld joints, the fixed mount and the area where the load is applied are represented as rigid elements connected into a single node. Rigid elements type **RBE2.** The following steps follow the example:

- 1. Select 1D options.
- 2. Select Rigid elements.
- **3.** Select the master (independent) node in the center of the load of fixing area.
- **4.** Select dependent nodes in the selected areas.
- 5. Select Create.



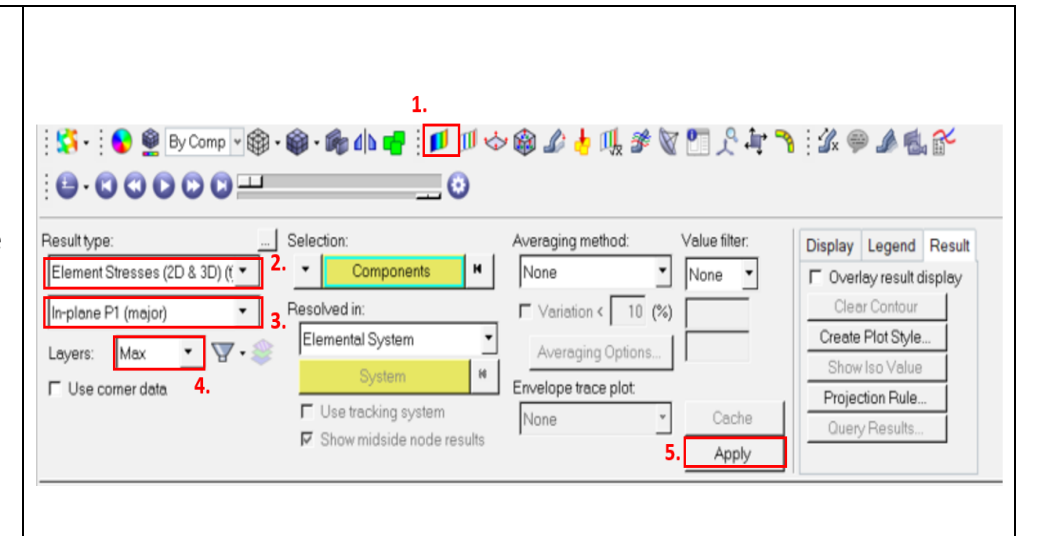


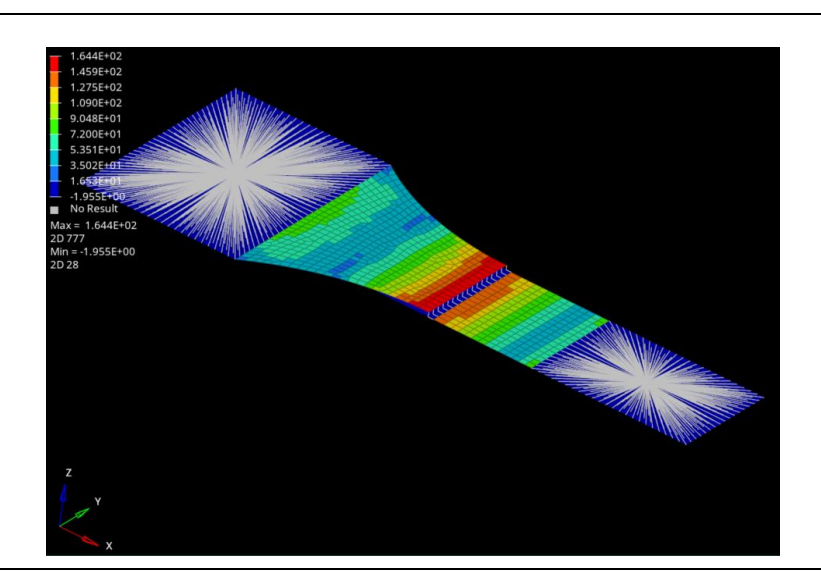


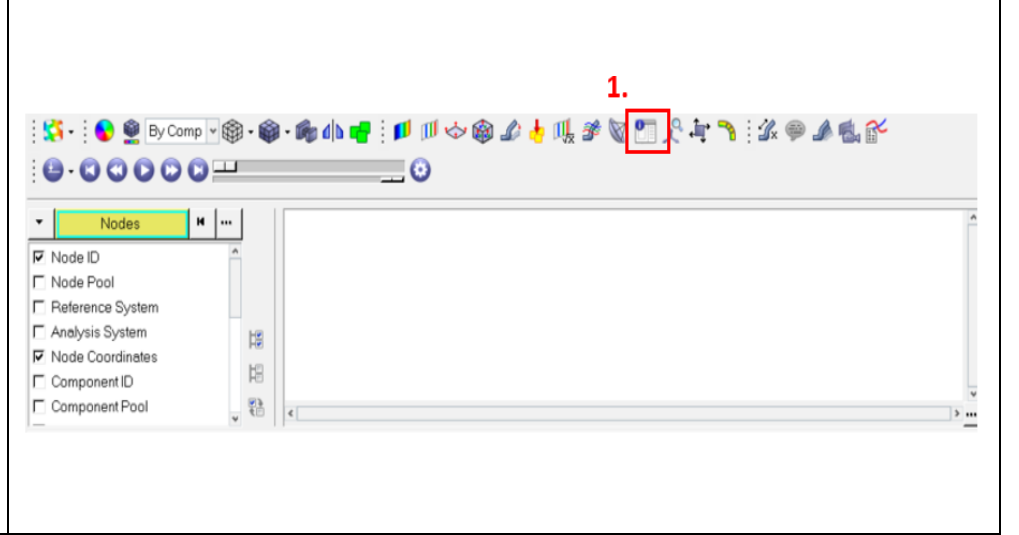
Selecting the Results button in the simulation monitor will open the hyperview window where the results are displayed.

- 1. Select the Contour button.
- **2.** Select "Element Stresses" as the result type.
- **3.** Specify the stress type; in this case, in-plane p1 is the principal maximum in-plane stress.
- **4.** Select the shell layer you want to analyze; in this case, the maximum.
- 5. Select Apply.

Select the Query button and select an element where the higher stresses in the welding zone are located to extract the maximum principal stress that will be used with the SN curve from the tests to obtain the approximate number of cycles to failure. In case of multiaxial loading, the maximum, minimum, ox and oy stresses are extracted to obtain the equivalent stress that will be compared to the teq-N curve to obtain an approximate number of cycles to failure





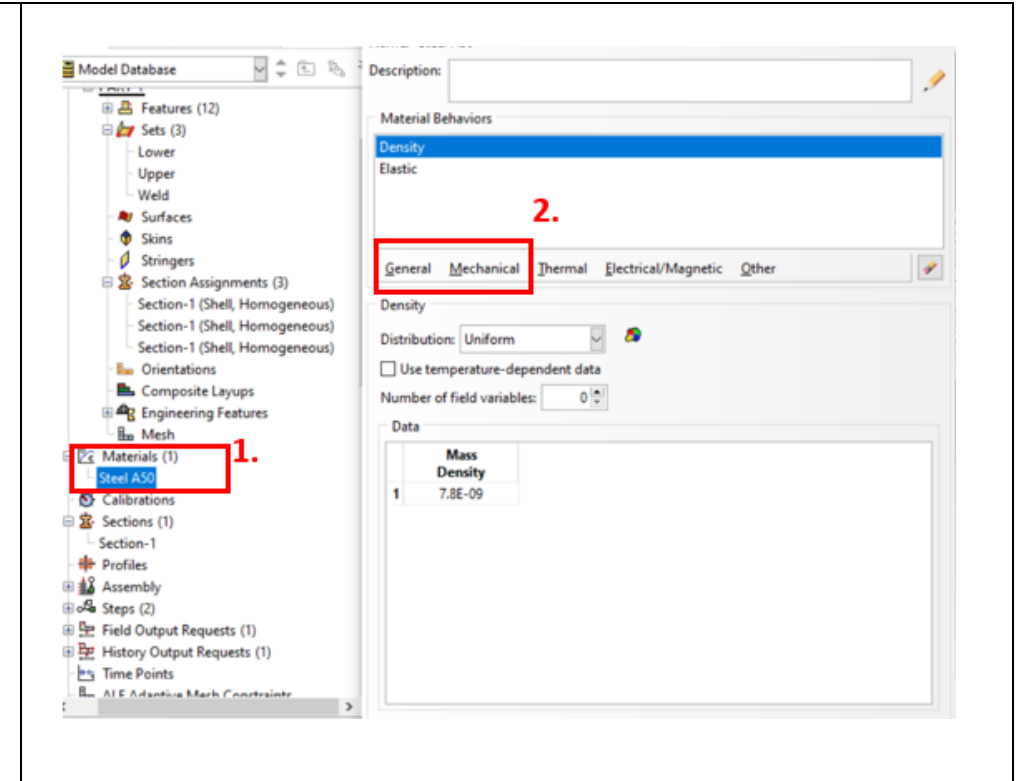


Abaqus

Description **Image** To import the model, whether an 1. external mesh or a geometry, you File Model Viewport View must: ew Model Database Ctrl+O Open... Network ODB Connector 1. Select File Close ODB... 2. In Import, select Part or Set Work Directory... **Assembly** if it's a geometry, or Ctrl+S Save As... Model if it's an external mesh, Compress MDB... which in this case was selected Save Display Options... Save Session Objects... because it was created in Load Session Objects... Optistruct. Sketch... Export Part... Bun Script... Assembl Macro Manager... Ctrl+P Print... Abaqus PDE... 1 D:/Santi (D)/.../Fx/LapFx.cae 出人人 2 D:/Santi (D)/.../TFz/T90Fz.cae 3 D:/Santi (D)/.../TFy/TFy2mm.cae 4 D:/Santi (D)/.../T90Fy/T90Fy.cae Constraints (36) In case of importing a geometry instead of a mesh, it must be Mesh Model: Module: created in the meshing module, where the Fayard rule parameters Part are defined. Property Assembly 1. Select Mesh in the Module Step section. Interaction 2. Select Global Seeds to define Load the element sizes, maintaining the Mesh rule for the size of elements close Optimization to the weld as the weld leg length. Job 3. Select Mesh Controls and define Visualization **QUAD** or **QUAD** Dominated. Sketch

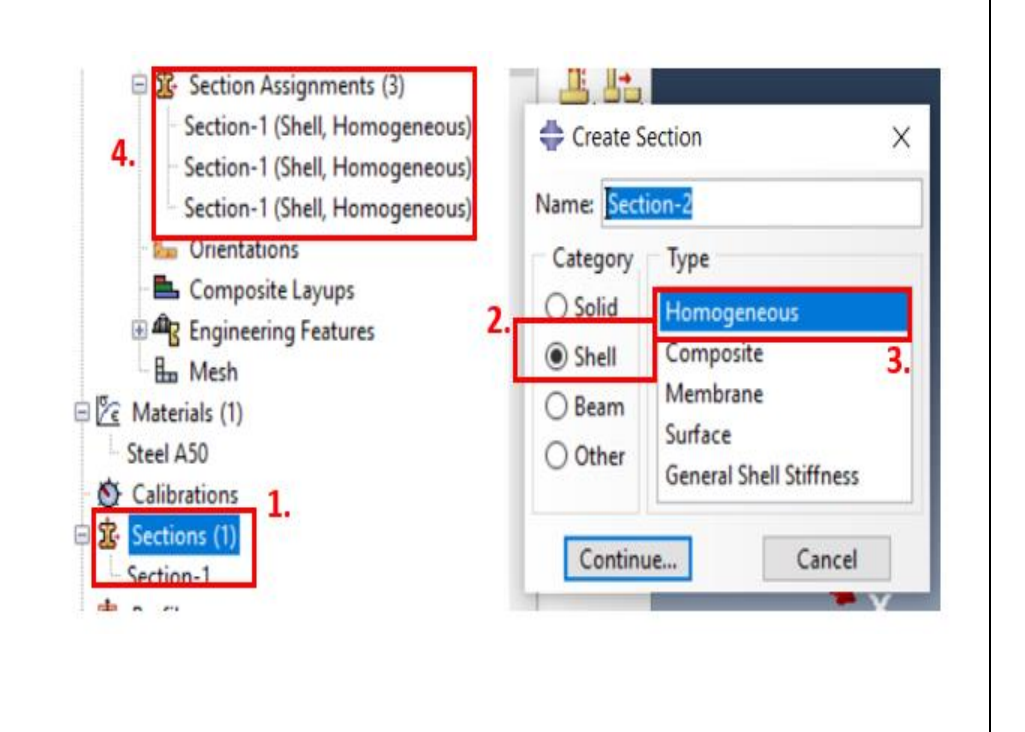
Define the basic material properties, including Young's modulus, Poisson's ratio, and density. These properties are essential for calculating stress and strain distributions within the components.

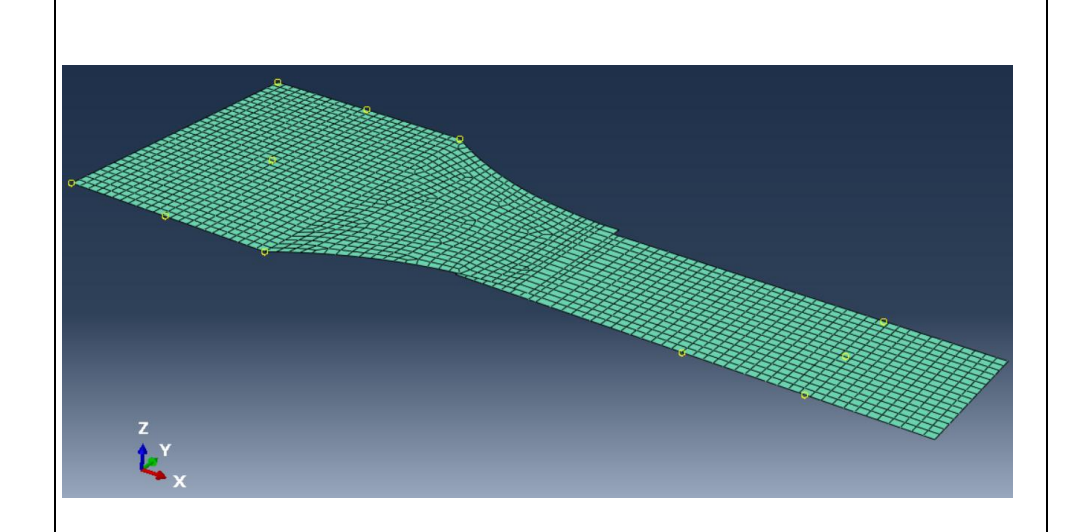
- **1.** Right-click on Materials in the Model tree and select Create.
- **2.** Select General and Mechanical properties.
- **3.** Add the basic Material properties (**E, NU, RHO**).



Define thesections of the components, which in this case must be defined as shells.

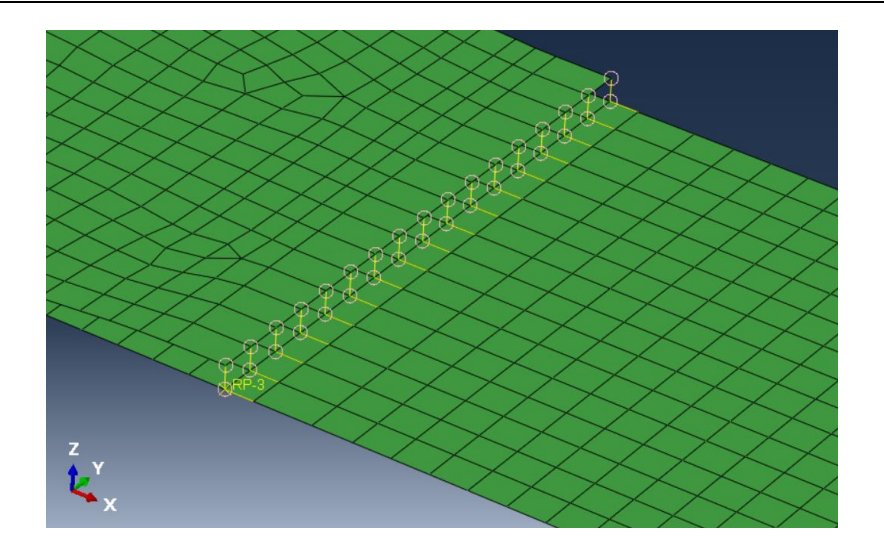
- **1.** Right-click on Sections in the Model tree and select Create.
- 2. Select Shell category
- **3.** Select **Homogeneous**, then add the surface thickness and assign the material.
- **4.** Go to **Section Assignments** in the Part section and assign the created section to each component



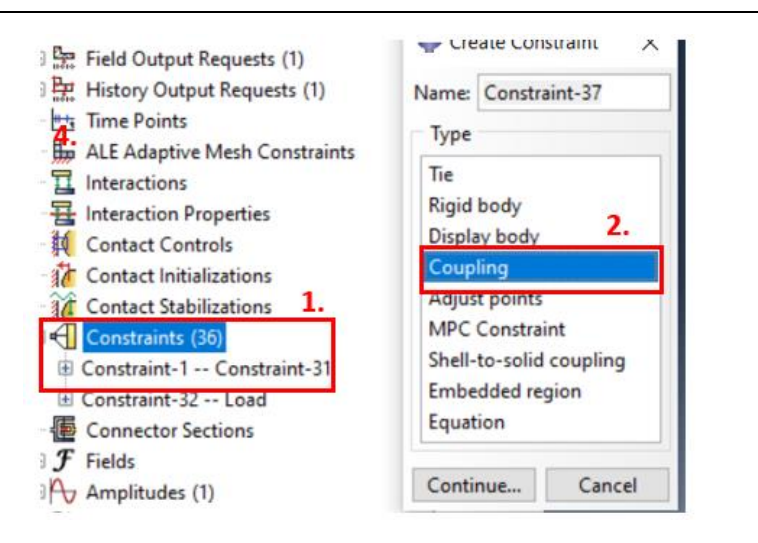


To create the weld representation, rigid elements type RBE2, known as Kinematic Couples in Abaqus, are the most appropriate choice since it gives the necessary rigidity that is formed by the weld. Such elements allow the transmission of stresses through the components.

- **1.** Select Constraints and create new.
- 2. Select Coupling.
- **3.** Select the independent node.
- **4.** Select the dependent node to connect both parts.

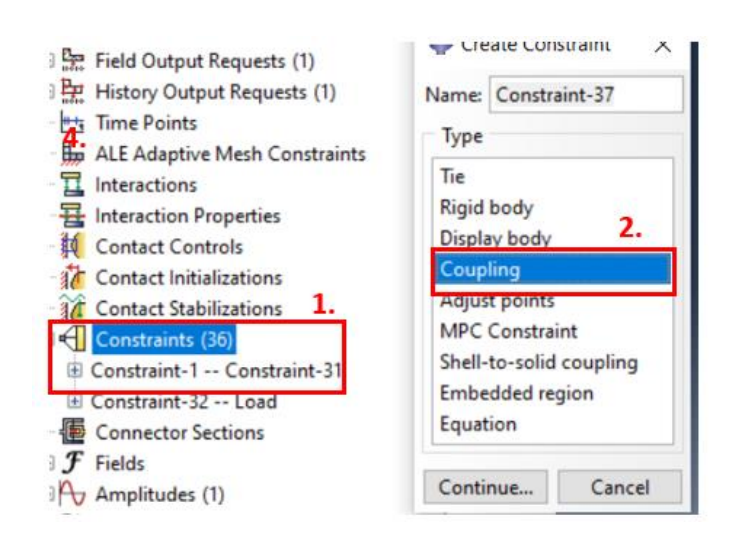


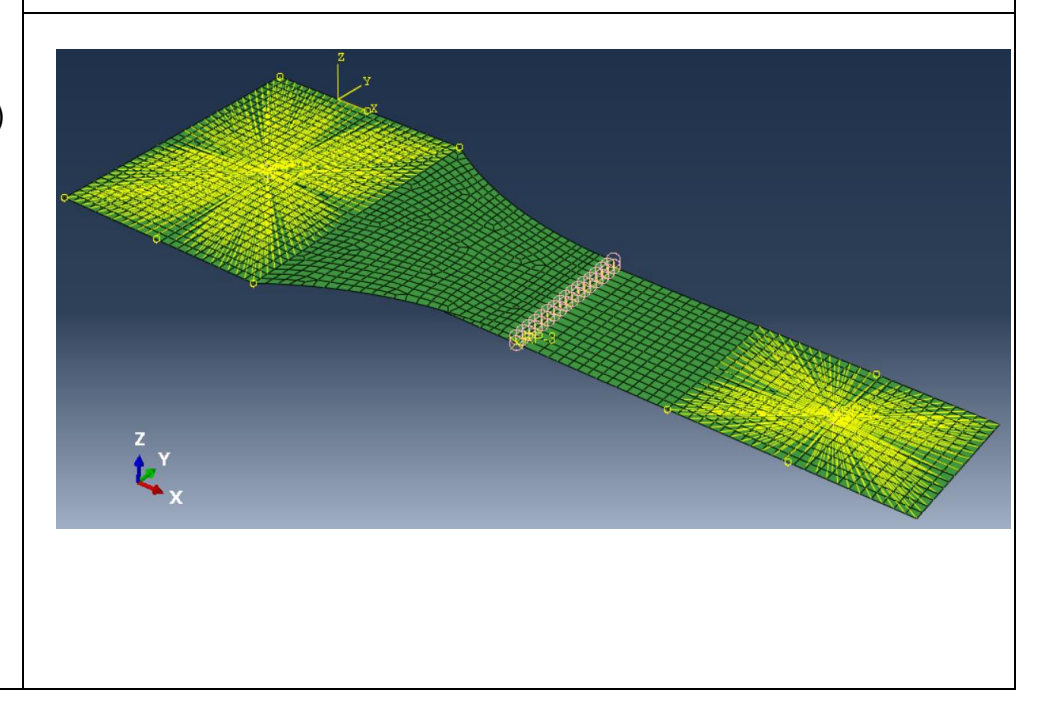
- **5.** Select Kinematic as type of coupling.
- **6.** Repeat until the nodes between both sections are connected.

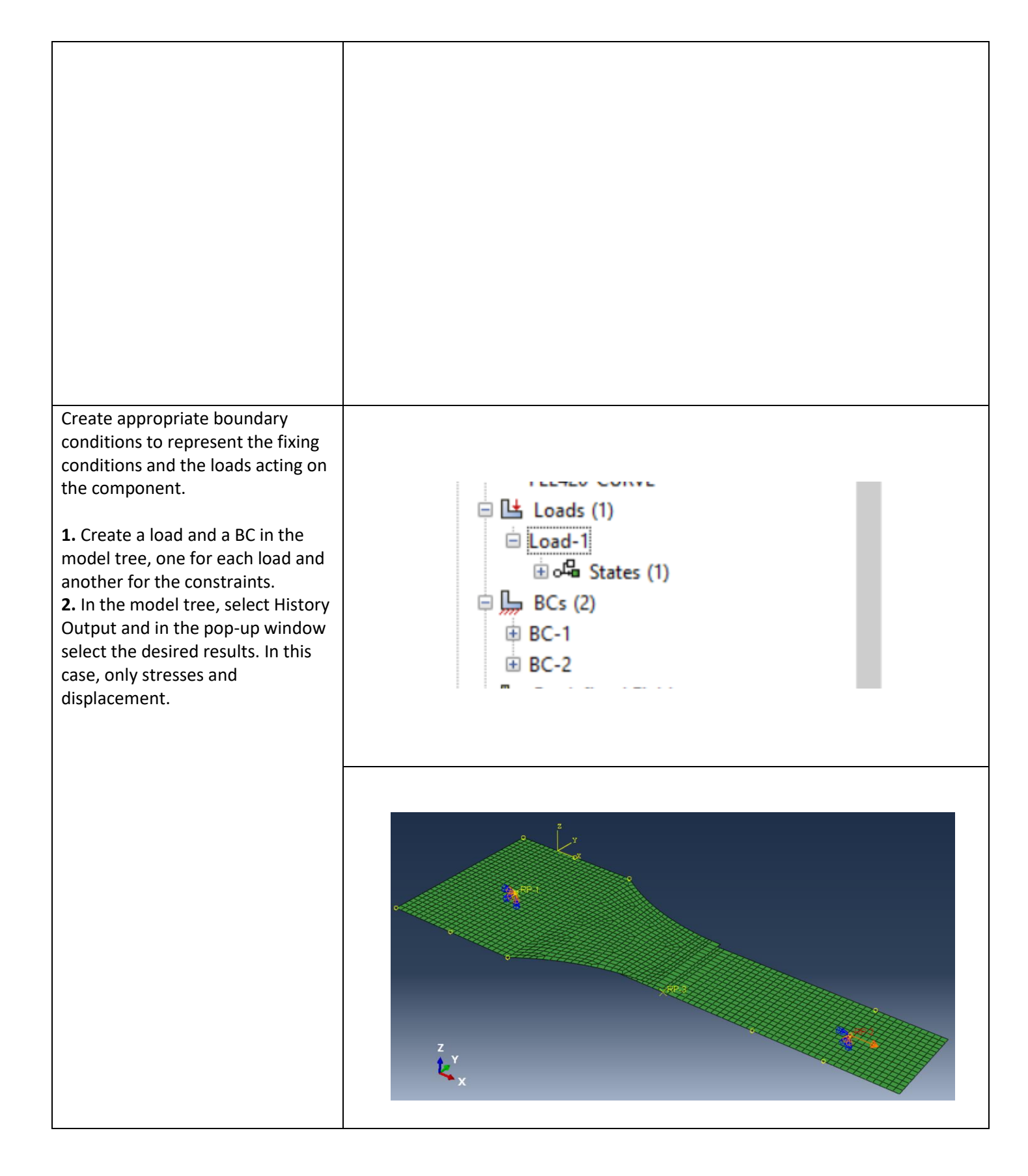


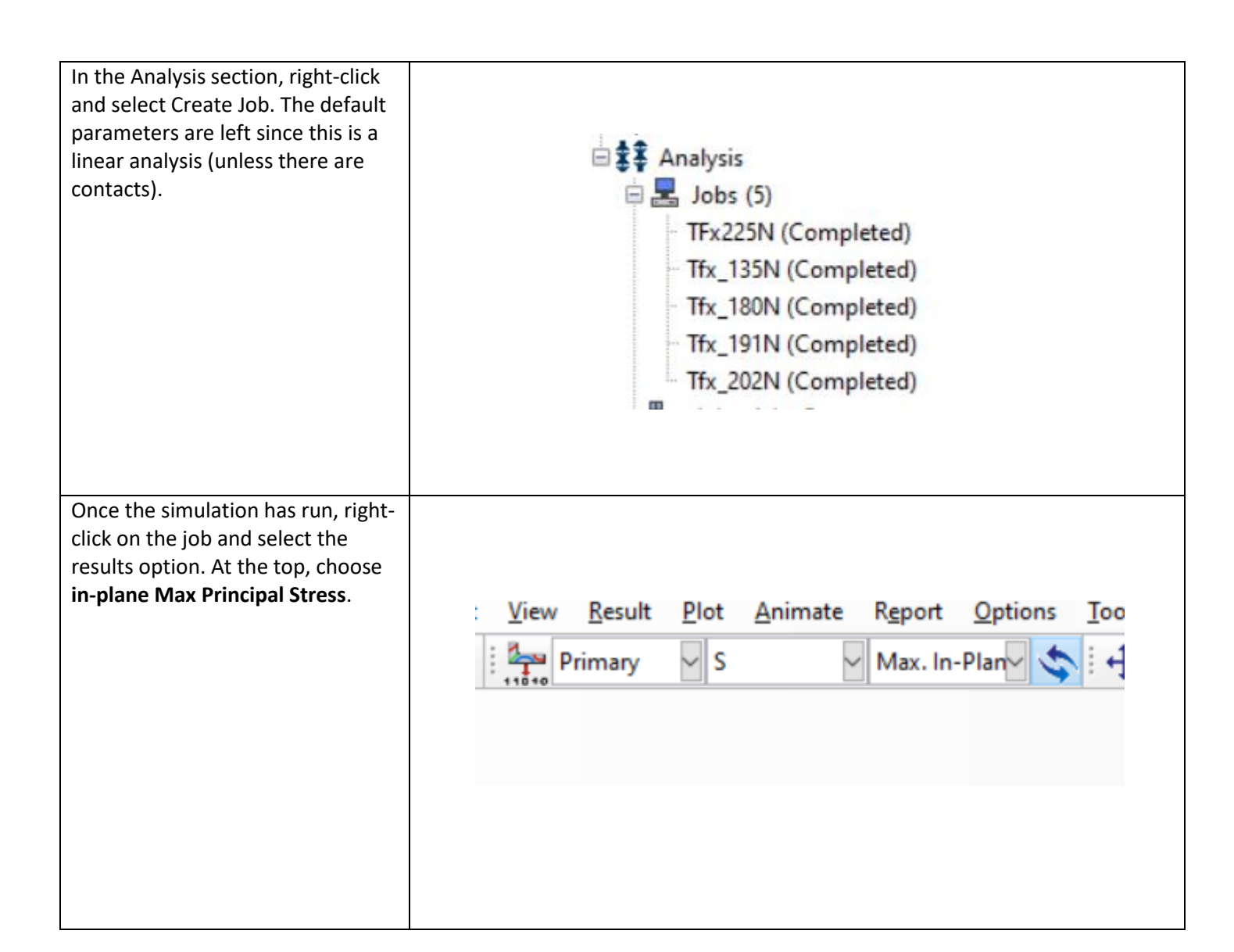
Create appropriate boundary conditions to represent the fixing conditions and the loads acting on the component. In this example, using one of the lap weld joints, the fixed mount and the area where the load is applied are represented as rigid elements connected into a single node. Rigid elements type RBE2, known as Kinematic Couples in Abaqus. The following steps follow the example:

- **1.** Select Constraints and create new.
- 2. Select Coupling.
- **3.** Select the master (independent) node in the center of the load fixing area.
- **4.** Select dependent nodes in the selected areas.
- **5.** Select Kinematic as the type of coupling.









To analyze the maximum stresses, it is necessary to observe the different layers of the shell. To do this, section points and **SNEG** or **SPOS** must be selected, depending on which has the highest stresses. Finally, the element stress can be extracted with the query option, which will be used with the **SN** curve from the tests to determine the approximate number of cycles to failure.

